



Osteoinductive composite coatings for flexible intramedullary nails



E.N. Bolbasov^a, A.V. Popkov^b, D.A. Popkov^b, E.N. Gorbach^b, I.A. Khlusov^{a,c,g}, A.S. Golovkin^d, A. Sinev^d, V.M. Bouznic^e, S.I. Tverdokhlebov^{a,*}, Y.G. Anissimov^f

^a Tomsk Polytechnic University, 30 Lenin Av., Tomsk 634050, Russian Federation

^b Federal State Budgetary Institution "Russian Ilizarov Scientific Centre", "Restorative Traumatology and Orthopaedics" of Ministry of Healthcare the Russian Federation, 6, M. Ulyanova Str., Kurgan 640014, Russian Federation

^c Siberian State Medical University, 2 Moskovsky trakt, Tomsk 634050, Russian Federation

^d Federal Almazov Medical Research Centre, 2 Akkuratova Str., 197341 St. Petersburg, Russian Federation

^e All Russian Scientific Research Institute of Aviation Materials, 17 Radio Str., Moscow 105005, Russian Federation

^f Griffith University, School of Natural Sciences, Engineering Dr., Southport, QLD 4222, Australia

^g Immanuel Kant Baltic Federal University, 14 A. Nevskogo Str., Kaliningrad 236041, Russian Federation

ARTICLE INFO

Article history:

Received 7 June 2016

Received in revised form 31 October 2016

Accepted 14 February 2017

Available online xxxx

Keywords:

Vinylidene fluoride – tetrafluoroethylene

copolymer

Piezoelectric

Flexible intramedullary nail

Hydroxyapatite

ABSTRACT

This work presents composite coatings based on a copolymer of vinylidene fluoride with tetrafluoroethylene (VDF-TeFE) and hydroxyapatite (HA) for flexible intramedullary nails (FIN). The effect of the proportion of VDF-TeFE (100–25% wt.) on physicochemical and biological properties of the composite coatings was investigated. It was shown that a decrease of VDF-TeFE in the coating hinders its crystallization in β and γ forms which have piezoelectric properties. The decrease also reduces an adhesive strength to 9.9 ± 2.4 MPa and a relative elongation to $5.9 \pm 1.2\%$, but results in increased osteogenesis. It was demonstrated that the composite coatings with 35% VDF-TeFE has the required combination of physicochemical properties and osteogenic activity. Comparative studies of composite coatings (35% VDF-TeFE) and calcium phosphate coatings produced using micro-arc oxidation, demonstrated comparable results for strength of bonding of these FINs with trabecular bones (~ 530 MPa). It was hypothesized that the high osteoinductive properties of the composite coatings are due to their piezoelectric properties.

© 2017 Published by Elsevier B.V.

1. Introduction

The work of doctors Prevot, Lascombes, and Metaizeau to optimize fixation of bone fragments in fractures of the femoral shaft, brought together the advantages of external and internal fixation in the method later dubbed Elastic Stable Intramedullary Fixation (ESIF) [1]. The technique is based on the introduction of pre-curved flexible intramedullary nail (FIN) into the intramedullary canal of the injured bone (Fig. 1a). In this way, a FIN, being in a mechanically stressed state, fixes a broken bone at three sites providing four types of fixation: bending, axial, translational and rotational [2]. Due to such advantages as the absence of damage to the epiphyseal plate, the preservation of contact between the muscle and the bone and the absence of significant blood loss, the method allows rapid consolidation of the fracture with minimal complications [3].

The combination of the ESIF method with a circular external fixator such as the Ilizarov [4] (Fig. 1b), reduced the Healing Index for lengthening the tibia in patients with Ollier's disease from 25 to 12 days [5]. This method also reduced the likelihood of complications in the forearm

extension [6] and correction of deformities in patients with melorheostosis [7].

It had been established that calcium phosphate coatings (CaP) on implants stimulate the attachment and differentiation of bone marrow multipotent mesenchymal stem cells (MMSC) into the osteoblasts [8, 9]. This effect can be used to produce bone tissue on the FIN surface in the intramedullary canal and increase bone mineralization and strength [10]. FINs with CaP coatings augment the fixation stability of bone fragments and accelerate the repair of tibial shaft fractures [11]. They are also used for the prevention of secondary orthopedic complications in children with X-linked hereditary hypophosphatemic rickets [12].

Thus, the micro-arc oxidation (MAO) method is used to create CaP coatings on the surface of the FIN. Such CaP coatings, which have high porosity and a high surface area, are soluble in physiological fluids, saturating the implantation site with calcium and phosphorus, and also possess high osteoinductive and osteoconductive properties [13]. One of the main disadvantages of these coatings is their low elasticity, causing delamination and destruction of the coatings due to significant bending deformations which the FIN undergoes during both the implantation and the operation. Another disadvantage of these coatings is that they can form only on the surface of the gate metal group (Ti, Zr, Nb, etc.) [14], which significantly reduces the clinical capabilities of

* Corresponding author.

E-mail address: tverd@tpu.ru (S.I. Tverdokhlebov).

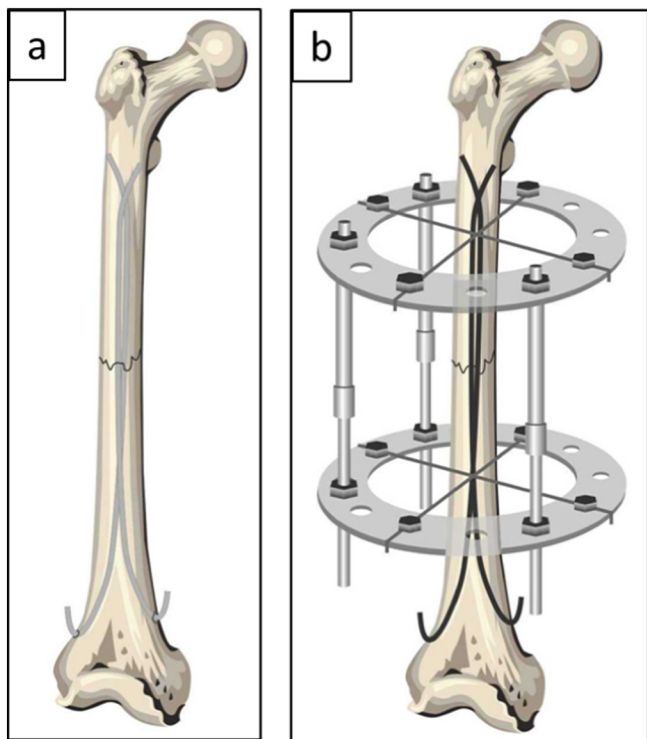


Fig. 1. Implantation scheme of FIN for classic ESIF (a) and ESIF combined with a Ilizarov frame (b).

the combined method, as the osteosynthesis often requires the use of stainless steel [15–17].

Thus, improved clinical outcomes and the expansion of using the combined osteosynthesis technique for various indications are associated with the creation of elastic CaP coatings on the FIN surface which are made from different materials. Such coatings have to produce bone tissue effectively in the intramedullary canal.

Bone tissue is a natural composite material of inorganic (Hydroxyapatite, HA) and organic (fibrillar protein - collagen) phases. Composite bone structure provides a unique combination of strength, elasticity and porosity [18]. In addition, bone is an electrically active structure in which electric potentials arise during deformation as well as exposure to electromagnetic fields [19]. Bone tissue exhibits piezoelectric (forward and reverse effect) [20,21], ferroelectric [22] and electrokinetic properties [23]. It is believed that under *in vivo* conditions the dominant mechanism of electrical activity in bone is due to electrokinetic processes, and electrical potentials generated by bone are, by nature, streaming potentials [24]. It is well accepted in the literature that for the most efficient bone formation, the properties of artificial substrates must be as close to the natural bone properties as possible [25]. Thus, the most effective coating for FINs is a composite, having a full set of required structural, chemical, and electrical properties. The use of piezoelectric materials can create composites providing an electrostimulating effect on the bone production as a result of the mechanical action on the composite [26].

The stimulating effect of an electric field on bone tissue formation has a direct and indirect nature. The direct effect is through exposure on intracellular components, such as ions, growth factors and receptors, and the indirect effect is due to change in protein conformation [27]. It is known that exposure to an electric field causes a redistribution of free calcium cations (Ca_2^+) in an extracellular and intracellular matrix, which stimulates the galvanotaxis of cells [28]. Direct electric fields are assumed to mobilize Ca^{2+} and Mg^{2+} towards the cathode or negatively charged surface, causing apatite formation, which can become a scaffold for bone formation by osteoblasts [29]. Since some extracellular

matrix proteins play multiple critical roles in cellular attachment, more adhered proteins on the surface could improve cellular adhesion and outgrowth. Electrical stimulation could result in more favorable conformational changes in fibronectin, which facilitates the adsorption of more proteins onto the biomaterial [30]. Electric fields aggregate charged ions and macromolecules in the bone interstitial fluid, which results in enhanced osteoblast activity [31,32]. Piezoelectric composites do not require the implantation of electrodes or batteries (which excludes the possibility of accumulation of the products of electrolysis in the tissue) and do not need external sources of energy to stimulate bone formation [26].

The development of piezoelectric composites for bone tissue regeneration is the subject of study amongst many research groups around the world. Two main directions in the development of this research can be identified. The first is directed at using piezoelectric materials with high piezoelectric coefficient values (as the inorganic phase). Currently, the most studied materials are based on barium titanate (BT, BaTiO_3) [33–36], composites of BT with HA [37–40], as well as composites of BT with biodegradable polymers [41,42] and polymer piezoelectric materials [43–45]. The possibility of using such piezoelectric materials as lithium niobate (LiNbO_3) [46,47], potassium and sodium niobate ($(\text{K}_x\text{Na}_x)\text{NbO}_3$) [48] and composites based on them [49] is under investigation. One of the factors limiting the use of inorganic piezoelectric materials for bone tissue regeneration is the risk of forming toxic ions and complexes [50,51], which may provoke adverse tissue reactions during a prolonged operation of the implant *in vivo*. The second direction is using piezoelectric polymer materials as the organic phase of the composite material [52–54]. Poly(vinylidene fluoride) (PVDF) and its copolymers with trifluoroethylene (VDF-TrFE) and tetrafluoroethylene (VDF-TeFE) are the most electroactive polymers [55]. Previously, it was shown that the films and nonwoven materials of PVDF in the β -phase can be used in active tissue engineering [56], because this phase promotes the differentiation of mesenchymal stem cells into osteoblasts [57–59] and accelerates the regeneration of bone tissue [60,61].

The ferroelectric and piezoelectric properties of PVDF occur because of dipole moments, which are perpendicular to the polymer chain axes, arising from significantly higher electronegativity of fluorine atoms, as compared with the hydrogen and carbon atoms [62,63]. However, the use of PVDF as an active composite for FIN coating is limited by its low adhesion. Increasing the adhesion usually requires the coating to be formed at temperatures above the melting point of PVDF, which leads to the formation of a paraelectric phase [64].

It is known that the introduction of >7 mol% of TeFE into the molecular structure of PVDF causes crystallization from the melt phase into the electrically active (ferroelectric) phase [65–69]. Thus, the direct crystallization from the melt into ferroelectric phase allows the use of the VDF-TeFE copolymer for the development of electrically active composite coatings for FIN. The VDF-TeFE copolymer is a non-toxic, biocompatible polymer [70,71], highly soluble in organic solvents such as acetone, methyl ethyl ketone, butyl acetate and ethyl acetate at room temperature [72,73]. This reduces the risk of rejection of the implant and simplifies the technological process of forming a composite material.

The aim of this work was to obtain a composite coating material which is based on a copolymer of VDF-TeFE and investigate its structure and properties, *in vitro* and *in vivo*, depending on the amount of bioactive filler. It also aims to provide a comparative assessment of the ability of FINs with the developed composite coating to stimulate the regeneration of bone tissue in ESIF conditions and compare new coatings to the uncoated metal FINs and FINs with bioactive ceramic coating produced by micro-arc oxidation (MAO) technology. Within the framework of comparative studies, uncoated metal FINs and FINs with bioactive ceramic coating produced by MAO technology were used as negative and positive controls respectively. Selection, as a positive control of FINs with bioactive ceramic coating produced by MAO, is due to their proven high clinical efficacy.

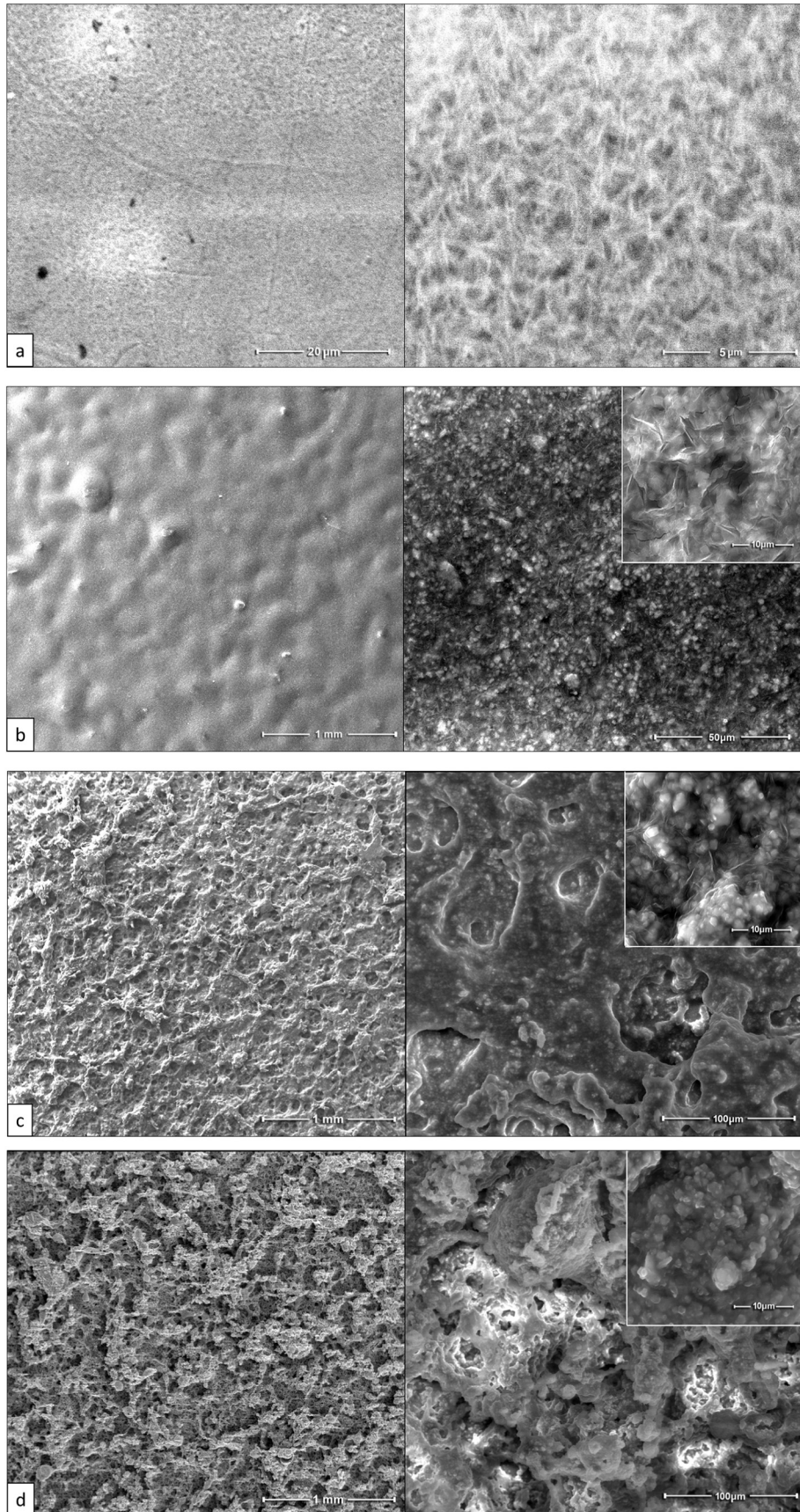


Fig. 2. SEM images of the samples surface (at different magnifications) with pure VDF-TeFE (a), 50% (b), 35% (c) and 25% (d) of VDF-TeFE.

2. Materials and methods

2.1. Preparation of the composite material

Composite coatings were produced using 6% solution of a random copolymer of VDF-TeFE containing 20 mol% of TeFE (HaloPolymer, Russia) in an organic solvent mixture of 20 wt% acetone and 80 wt% ethyl acetate. Preparation of a copolymer VDF-TeFE solution was carried out in a sealed reactor at room temperature and constant stirring until a homogeneous clear solution is formed.

HA powder and ethyl acetate (50/50 wt%) were placed in sealed glass container and the powder was dispersed in ethyl acetate using ultrasonic unit (Sapphire 5M, Russia) for 8 h. The VDF-TeFE copolymer solution was added to the resulting dispersion so that the weight amount of the VDF-TeFE copolymer in the composite was 50%, 35% and 25% all by wt%. The resulting mixture was further treated for 12 h using an ultrasonic device at power setting 150 W (Sapphire 5M, Russia).

2.2. Formation of the composite coating

Formation of the composite coating was performed in two layers by using a pneumatic spray nozzle 4 Minijet (Sata, Germany) with diameter set to 1 mm, air pressure to 1.4 atm and the distance between the spray gun and the substrate to 20 cm.

The first layer (primer layer) coating was formed from 6% of a random copolymer of VDF-TeFE solution. After application of the primer layer the sample was placed in a chamber oven and heated to 200 °C at 2° per minute rate, followed by ageing for 30 min. The second layer of the dispersion of the HA powder in a copolymer of VDF-TeFE solution is when applied to the 200 °C heated sample. After the application of the second coat the final formation of the composite material was performed by heating to a temperature of 220 °C at 10° per minute then ageing for 30 min, cooling to 100 °C temperature at a rate of 2° per minute and ageing for 4 h and finally hardening in distilled water at 30 °C.

321 stainless steel was used for the substrate plates. To increase the adhesion the plate surface was roughened before application using corundum blasting, and then sequentially washed with trichloromethane (CHCl₃) and ethanol (C₂H₅OH) to remove contaminants.

2.3. Investigation of composite coatings

Morphology of composite coatings was investigated using scanning electron microscopy (SEM, Quanta 400 FEI, USA). Prior to SEM the surface of coating was covered with a thin layer (~30 nm) of gold, using a magnetron sputtering system SC7640 (Quorum Technologies Ltd., UK). Morphological characteristics of the coatings were measured using the software Image J 1.38 (National Institutes of Health, USA).

A study of open porosity of the composite coatings was performed using hydrostatic weighing method described in [74,75]. For the study, on the surface of the titanium disks with a diameter of 10 ± 0.1 mm and a height of 1.5 ± 0.1 mm the composite coatings were formed as described above.

Open porosity of the composite coatings (P) was calculated using Eq. (1)

$$P = \frac{(m_{dc}^a - m_d^a) - (m_{dc}^g - m_d^g)}{(m_{dc}^a - m_d^a) - (m_{dc}^l - m_d^l)} \times 100\%, \quad (1)$$

where m_{dc}^a is the mass of coated saturated disc weighed in air, m_d^a is the mass of uncoated saturated disc weighed in air, m_{dc}^g is the mass of coated dry disc weighed in air, m_d^g is the mass of uncoated dry disc weighed in air, m_{dc}^l is weights' mass that balances coated disc immersed in liquid, and m_d^l is weights' mass that balances uncoated disc immersed in liquid.

Isopropyl alcohol (Ecos-1, Russia) was used as the saturation liquid. Before measurement the composite coatings were dried in an oven (Labtech, Russia) at 115 ± 5 °C until constant weight was achieved. To

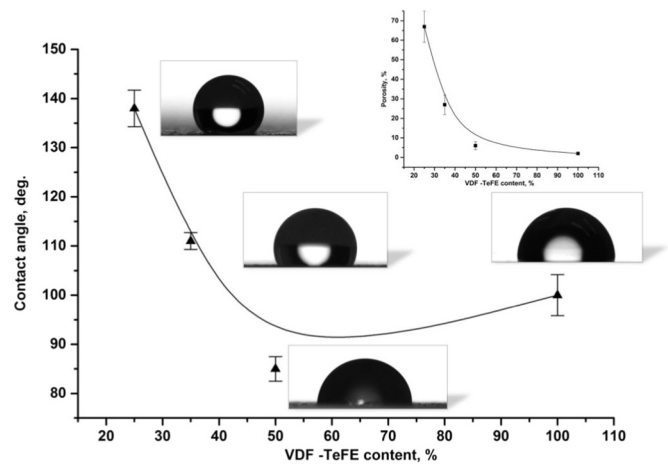


Fig. 3. Contact angles and porosities (insert) of the coatings vs the amount of the copolymer VDF-TeFE (with B-spline fitting as solid line).

saturate pores in the coatings the sample was placed into a container with isopropyl alcohol and incubated for three days. Analytical balance (Gosmetr, Russia) was used for the porosity study.

The elasticity of the composite material of 70 ± 10 μm thickness was investigated with bending device (Gradient-Techno, Russia) in accordance with ISO 1519. For the elasticity measurements the coatings were formed on the substrate plate (120 × 35 × 0.3 mm) made of stainless steel 321 as described above. The elasticity index of the coatings was selected as the smallest diameter of the rod, bending around which did not lead to mechanical failure, or delamination of the composite coating.

Adhesion of the composite coatings was studied according to ISO 13779-4 "Implants for surgery - Hydroxyapatite - Part 4: Determination of coating adhesion strength". The coatings for this study were formed on the substrate plate (40 × 20 × 2.5 mm) so that the total area of the coatings was 284 ± 7 mm. A steel plate (40 × 20 × 2.5 mm) without coating was then glued to the coating using Scotch-Weld 2214-NMF (3M, USA). The plates were then pressed together at 0.14 ± 0.01 MPa and placed in an incubator at 90 °C for 48 h. Studies were conducted using the testing machine Instron 3369 (Instron, UK) at a crosshead speed of 2.5 mm per minute.

Surface wettability was measured using a contact angle meter (Easy Drop, Germany). 3 μl of milli-Q water was placed on the coatings and the measurement was taken after 1 min.

It is known that direct observation of ferroelectric properties (ED hysteresis loop) for the PVDF and its copolymers is possible in the electric field strength of 40 mV/m [76], which requires obtaining homogeneous samples without defects to avoid electrical breakdown [77] [78]. The composite material used in this study contains a significant number of defects resulting from the introduction HA particles into the polymer structure, which reduces its dielectric strength. Ferroelectric properties of PVDF and its copolymers are determined by the conformation of macromolecules and as a result by its crystalline structure [79,80]. There are three main PVDF polymorphs (α, β, γ). α-Phase is characterized by a monoclinic lattice in which chain (TGTC⁻) conformation have opposite dipole moments, so in general it is

Table 1
Mechanical properties of composite coatings.

VDF-TeFE copolymer amount, wt%	Adhesive strength, MPa	Elongation, %	Elasticity index, mm
100	4.2 ± 1.8	3.6 ± 2.4	1
50	21.2 ± 3.6	35.3 ± 5.6	1
35	15.4 ± 1.8	16.3 ± 4.5	2
25	9.9 ± 2.4	5.9 ± 1.2	3

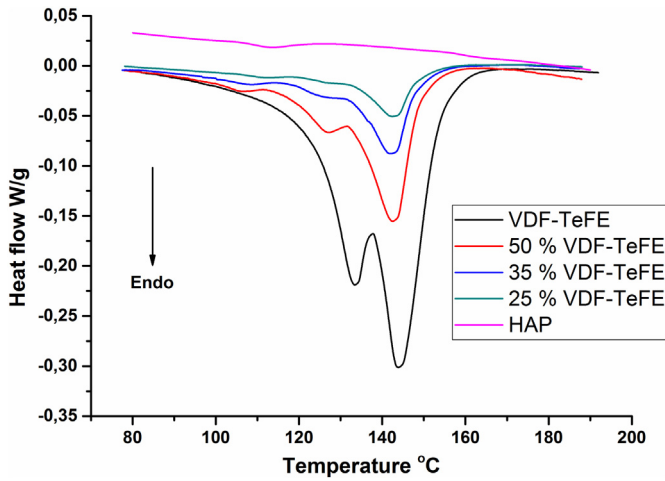


Fig. 4. DSC curves of the investigated samples.

nonpolar. γ -phase contains a weakly polar cell with a chain (T_3GT_3G -) conformation. β -phase is the most electroactive and is characterized by orthorhombic lattice with polar cell in which the chain has a planar zigzag (TTT) conformation [62,63]. The presence of polymorphic conformations and crystal structures typical of the paraelectric and ferroelectric phases allows to determine their presence, using techniques such as DSC, XRD and FTIR [81].

Differential scanning calorimetry (DSC) (SDT Q600, TA Instruments) was used to determine the heat of fusion (ΔH_{fm}) and thermal transitions, such as the Curie temperature (T_c) and the melting temperature (T_m), in composite materials. At the Curie temperature a unique solid–solid phase transition takes place before melting when the VDF–TeFE transforms from a ferroelectric (piezoelectric) to a paraelectric (non-piezoelectric) state. The calculated heat of fusion (ΔH_{ft}) for the composites can be found as [82]:

$$\Delta H_{ft} = \omega_m \Delta H_{fm}^{VDF-TeFE}, \quad (2)$$

where $\Delta H_{ft} = \Delta H_{fm}^{VDF-TeFE}$ is the measured heat of fusion of the film of the copolymer VDF–TeFE and ω_m is the copolymer weight proportion in the composite.

The change of the degree of crystallinity of the composite material compared with the theoretical value (ΔX_c) was calculated as:

$$\Delta X_c = \frac{\Delta H_{fm}}{\Delta H_{ft}} \quad (3)$$

The crystal structure of the coatings was investigated using X-ray diffraction analysis (XRD) (Shimadzu 6000, Japan). The samples were exposed to a monochromatic $\text{Cu K}\alpha$ (1.54056 Å) radiation. The accelerating voltage and the beam current were set to 40 kV and 30 mA respectively. The scanning angle range, scanning step size and signal collection time were 10–55°, 0.02° and 1.5 s respectively. The average size of the

crystals (l_c) was calculated using the Debye–Scherrer equation:

$$l_c = \frac{k\lambda}{\cos\theta\sqrt{\beta^2 - \beta_0^2}}, \quad (4)$$

where λ is the wavelength of the incident radiation, β the width of the reflection at half height, β_0 is the broadening reflex of the apparatus, θ is the angle of diffraction and $k = 0.9$.

The conformation of macromolecules was investigated by Attenuated Total Reflectance (ATR) Fourier Transform Infrared spectroscopy (FTIR) (Tensor 27, Bruker) with ATR attachment (PIKE MIRacle, Bruker) on the crystal ZnSe was used. Investigations were carried out in the spectral range of 500–2000 cm^{-1} with a resolution of 2 cm^{-1} .

2.4. Cell adhesion and viability

The study of cell adhesion and viability was conducted using adipose-derived multipotent mesenchymal stem cells (MMSC). MMSC were collected from healthy donors and immunophenotyping with flow cytometer GuavaEasyCyte6 (Millipore, USA) using CD19, CD34, CD45, CD73, CD90 and CD105 monoclonal antibodies (BD, USA) as previously described [83].

The viability of cells on the coatings surface was studied using flow cytometry with Guava Easy Cyte 6 (Millipore, USA) after cell incubation on the surface for 72 h. The cells were detached from the surface with 0.5% solution of trypsin–EDTA (Sigma Aldrich, USA), centrifuged for 10 min at 716g, resuspended in 1 ml of the culture medium and stained with Annexin V–FITC Apoptosis Detection kit (Sigma Aldrich, USA). For detection Annexin V – Propidium Iodid –, Annexin V + Propidium Iodid + and Annexin V + Propidium Iodid – were used for live, necrotic and apoptotic cells respectively.

The effectiveness of cell adhesion to the coatings was evaluated by fluorescent microscopy (Axio Observer, Carl Zeiss, Germany) as described earlier [84]. The effectiveness of cell adhesion was assessed by the number of adherent cells visible in ten fields of view of the microscope with the average normalised to 1 mm^2 .

The study was performed according to Helsinki declaration and approval was obtained from the local Ethics Committees in Almazov Federal Medical Research Centre. Written informed consent was obtained from all subjects prior to fat tissue biopsy. All tests were made in triplicate.

2.5. Ectopic osteogenesis test

To study the ability of composite materials to produce bone tissue in an in vivo system well known ectopic bone formation test [85] was used. For this test titanium disks with diameter 10 ± 1 mm were coated with the composite material as described above. On the formed coating the bone marrow, washed carefully by minimal essential medium (DMEM) (Sigma–Aldrich, USA) from the femur of mice CBA/CaLac, was applied in vitro as described in [86]. Investigations were carried out on 24 CBA/CaLac mice in compliance with the principles of humane treatment of laboratory animals set out in [87]. In this study 16 animals were used for the implantation and eight animals served as bone marrow donors.

Table 2

Calculated and measured heat of fusion of the materials.

VDF–TeFE copolymer amount, wt%	Measured heat of fusion of the composite material ΔH_{fm} , J/g	Calculated heat of fusion of the composite material ΔH_{ft} , J/g	Change in crystallinity compared with the theoretical value ΔX_c
100	31.3	31.3	1
50	10.1	15.8	0.64
35	6.0	10.9	0.55
25	4.5	7.3	0.62

The samples were incubated for 45 min at 37 °C in culture medium consisting of 95% DMEM (Sigma-Aldrich, USA) and 5% fetal bovine serum (Sigma-Aldrich, USA) to adhere the bone marrow. To determine the area covered by the bone marrow tissue each sample was photographed (PowerShot A 630, Canon) and the tissue area (μm^2) measured processing digital images with the program Image J 1.38 (National Institutes of Health, USA).

The sample was then implanted under the etherisation into the lateral subcutaneous pocket of the animal venter and the wound sutured. After 45 days the animals were sacrificed using the overdose of ether anaesthesia. Disks were explanted and the surface area occupied by the formed tissue determined as described above. Then implants were soaked in neutral formalin for 24 h to fix the formed tissue lamellae. After fixation, the samples were decalcified with 10% EDTA. Then the tissue lamellae were removed from the implants surface, dehydrated and embedded in paraffin for producing histological sections as usual technique. The cross thin (5–10 μm) sections were deparaffinised and stained with hematoxylin and eosin. To determine the type of tissue formed on the surface of the implant stained tissue sections of the middle part of the lamellae were examined histologically by standard method of light microscopy (Axioskop 40, Carl Zeiss, Germany). Formed bone tissue with or without bone marrow was considered in histological sections as a positive outcome of the ectopic osteogenesis test.

2.6. Comparative studies of the morphological features of the process of regeneration of bone tissue around the implanted FIN

Comparative experimental studies of the morphological features of the process of regeneration of bone tissue around the implanted FIN was performed on the in vivo in adult dogs. For this purpose, inclined holes with 3 mm diameter communicating with the bone medullary canal were formed with an awl in the proximal tibial metaphysis of a cortical bone. Through the hole the FIN was introduced into the medullary canal. The proximal end of the FIN was folded into a loop and is located under the fascia. After the FIN implantation soft tissues were sutured.

4 weeks after the implantation FINs were removed by pulling on the loop with dynamometer (DEPZ-1D-1U-1, Russia), measuring the required force. Calculation of FINs pull-off force (P) was carried by the equation:

$$P = \frac{F}{L \cdot d}, \quad (5)$$

where F is the breakout force, L is the length of the FIN and d is the diameter of the FIN.

After the removal of FINs portions of the bone metaphysis were sawed longitudinally and transversely, fixed in 10% neutral formalin and embedded in celloidin for histological studies. Histo-topographic sections were stained according to Masson's trichrome staining method as described in [88]. The study of reparative regeneration of bone tissue was performed by light microscopy using a microscope "Nikmed-5" (LOMO, Russia). For processing histological preparations hardware and software complex "DiaMorph" (Russia) mounted on a large research photomicroscope (OPTON, Germany) was used.

Studies were conducted on 9 adult dogs with the principles of humane treatment of laboratory animals set out in [87]. As a control, the steel K-wire without coating and titanium FIN with an osteoinductive coating made by MAO technology were used. Electrolyte solution based on phosphoric acid (H_3PO_4) with density ($\rho = 1.0824 \text{ g/ml}$) with 80 g/l of calcium carbonate and 70 g/l of HAP was used to produce MAO coatings. Coating formation was carried out using a pulse current for 5 min. The current had the pulse time of 50 μsec , pulse repetition rate of 100 Hz, initial current density of 0.2 A/mm^2 and end voltage of 300 V [89].

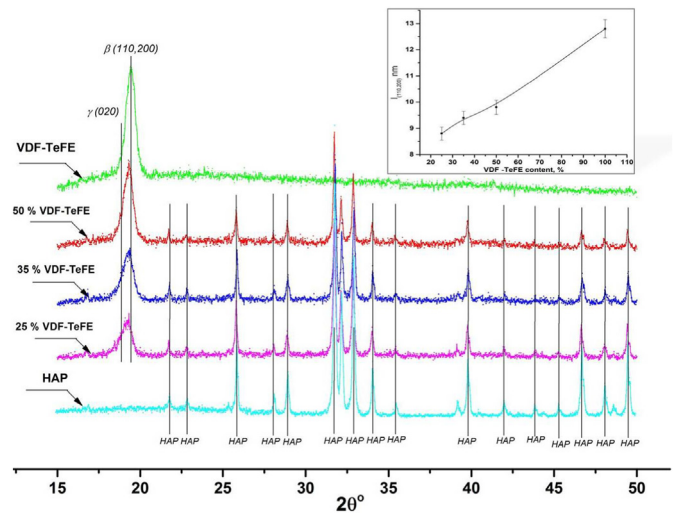


Fig. 5. XRD spectra of the investigated samples.

2.7. Statistics

The statistical analysis was performed in Statistica (StatSoft, Dell) software using Mann–Whitney test. The differences between groups were considered significant at a significance level of $p < 0.05$.

3. Results and discussion

Fig. 2 shows SEM images of the samples at different magnifications. At smaller magnifications, VDF-TeFE copolymer film has an appearance of a uniform smooth surface with low porosity (Fig. 2a). At significant magnifications, randomly distributed contrasting fibrillar structures with a length of $1.1 \pm 0.3 \mu\text{m}$ and a width of $0.19 \pm 0.04 \mu\text{m}$, are visible on the surface. Previously, the formation of fibrillar structures in the annealed non-oriented films of the copolymers VDF-TeFE and VDF-TrFE was observed by several authors [90–92], and is associated with the formation of crystalline regions of the electrically active β -phase formed in the film during high-temperature annealing.

Increasing the amount of HAP powder in the composite material causes a change in the structure of the composite material surface. When the amount of VDF-TeFE is 50% by weight, micro-relief in the form of "hills" and "valleys" with smooth rounded edges is apparent on the surface of the composite material (Fig. 2b). On the surface of the hills are particles of HA probably covered with a thin film of VDF-TeFE copolymer with numerous breaks (Fig. 2b). The open porosity of

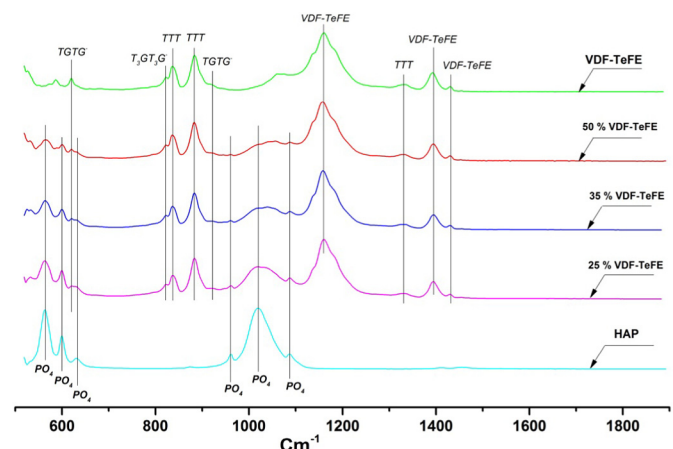


Fig. 6. FTIR spectra of samples.

Table 3Cytotoxic results of the samples tested using flow cytometry, $X \pm SD$.

Viability indicators	Cell control	VDF-TeFE 100%	VDF-TeFE 50%	VDF-TeFE 35%	VDF-TeFE 25%
Viable, %	92.5 \pm 0.3	91.4 \pm 0.8	90.8 \pm 1.4	90.9 \pm 1.7	91.5 \pm 2.0
Necrosis, %	3.4 \pm 0.3	3.7 \pm 0.7	4.7 \pm 0.7	3.5 \pm 0.6	3.3 \pm 1.0
Apoptosis, %	2.6 \pm 0.2	2.0 \pm 0.4	2.2 \pm 0.1	3.1 \pm 0.4	2.8 \pm 0.1

the composite material was <8%, and most likely due to the porosity of HA particles.

Reducing VDF-TeFE copolymer concentration in the composite material to 35% leads to the formation of a significant number of macropores with an average diameter of $130 \pm 75 \mu\text{m}$ (Fig. 2c). At the base of the macropores there are smaller micropores with an average diameter of $3.1 \pm 0.8 \mu\text{m}$, with HA particles extruding from the composite surface (Fig. 2c) with an overall porosity of $26 \pm 4\%$.

Further reducing the VDF-TeFE copolymer concentration to 25% increases the size of the micropores of the composite material to $153 \pm 26 \mu\text{m}$ (Fig. 2d) and micropores to $8.5 \pm 4.7 \mu\text{m}$ (Fig. 2d). The porosity of the composite material increased to $67 \pm 8\%$. Significant number of HA particles, loosely associated by polymer material, was observed on the surface of the composite material (Fig. 2d).

Results of the wettability study with distilled water on the coatings are shown in Fig. 3. The water contact angle of with the copolymer VDF-TeFE film was $100 \pm 4^\circ$.

The high value of the contact angle, and as a consequence, the high hydrophobicity of the coating is due to the high electronegativity of fluorine atoms, which is a distinct feature of fluorinated polymer materials [80]. Reducing the VDF-TeFE copolymer concentration in the composite material to 50% leads to a decrease in the contact angle to $85 \pm 3^\circ$, which is the result of a uniform topography and the presence of HAP particles on the surface of the composite [93]. Further reducing the

VDF-TeFE copolymer concentration to 35 and 25% leads to an increase in the contact angle to $111 \pm 2^\circ$ и $138 \pm 4^\circ$. The increase in the contact angle of the coatings has a strong relationship with the increase in their porosity (Fig. 3 inset). It has been previously shown that porous surfaces have substantially higher contact angle values [94]. Thus, a significant increase in the contact angle of the composite material, with a decrease in the proportion of the hydrophobic copolymer VDF-TeFE, is likely due to an increase in the porosity of the composite coatings.

The parameters describing mechanical properties of the composite coatings are shown in Table 1. In the study of adhesion of composite materials, cohesive destruction of the coatings was observed, which indicated a high adhesiveness of the samples. The composite copolymer containing 50 wt.% VDF-TeFE had the greatest strength, elongation and elasticity of all the composite materials. Increasing the HA amount resulted in a significant decrease in a cohesive strength and elongation, which is associated with an increase in the porosity of the coatings and the deterioration of ties between the HA particles due to the decrease in the amount of VDF-TeFE copolymer.

Low levels of strength and elongation of the pure VDF-TeFE coatings are likely linked to their low surface energy and roughness which significantly hinder the formation of adhesive bonds between the epoxy and the fluorinated plastic surface.

Fig. 4 presents DSC curves for the samples. In the DSC curve for the coating derived from a pure VDF-TeFE polymer solution, there are two overlapping intense endothermic effects, first near 132°C and the second around 143°C . The first endothermic effect corresponds to the Curie transition and the second effect corresponds to the melting of the copolymer VDF-TeFE. This curve is characteristic of VDF-TeFE copolymer samples with a high β ferroelectric phase proportion [95]. The curves for HA powder and the composite materials both have a weak endothermic effect in the region of $108\text{--}115^\circ\text{C}$ due to the removal of weakly bound water. Increasing the amount of HA in the composite material reduces the heat of fusion of the composite materials, and the

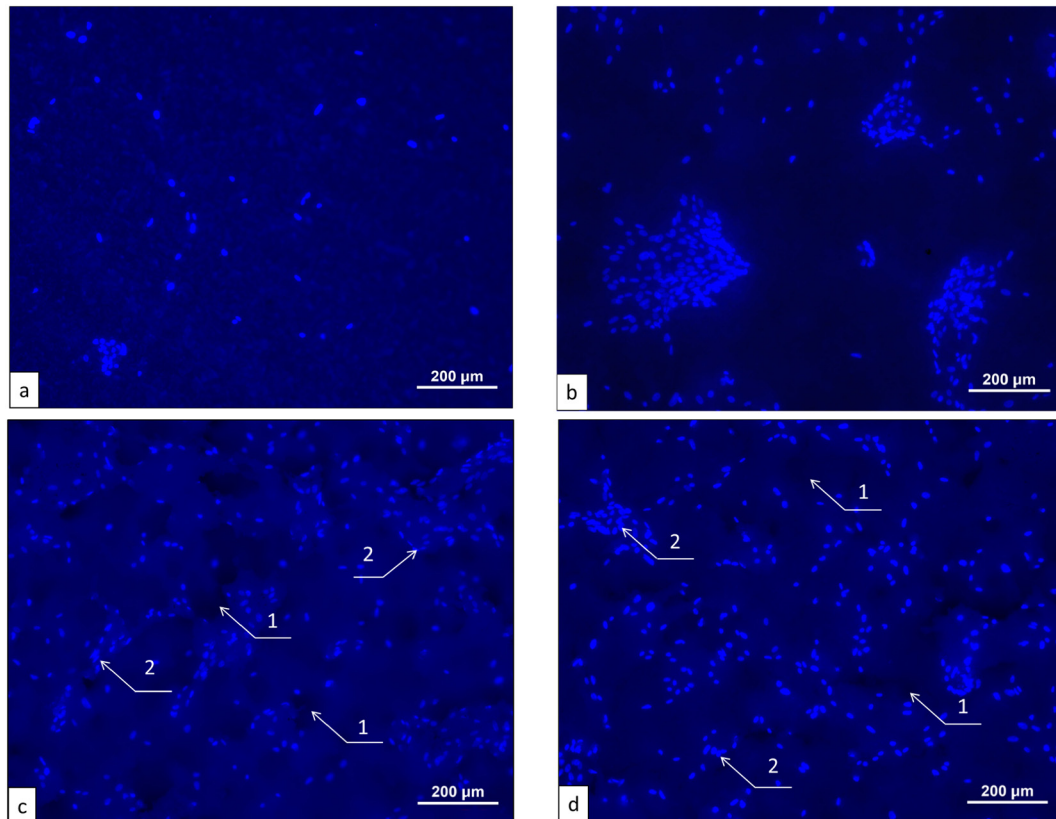


Fig. 7. Fluorescence microscopy of the surfaces of samples with adhered cells for pure VDF-TeFE (a), 50% VDF-TeFE (b), 35% VDF-TeFE (c) and 25% VDF-TeFE (d). Arrows marked 1 and 2 point to pores and DAPI stained nuclei.

Table 4
The number of adherent cells on the sample surface, $X \pm SD$.

Sample	VDF-TeFE 100%	VDF-TeFE 50%	VDF-TeFE 35%	VDF-TeFE 25%
Amount of adipose-derived MMSC on 1 mm ² of the surface	59 ± 7	337 ± 30*	290 ± 20*	318 ± 26*

* $p < 0.05$ significance level from VDF-TeFE 100%.

degree of crystallinity of the copolymer VDF-TeFE is smaller than the calculated value (Table 2). This indicates a negative influence of the HA powder on the process of copolymer VDF-TeFE crystallization. The decrease in the degree of crystallinity, with an increase in the amount of inorganic fillers in the fluorocarbon ferroelectric polymers, was noted previously [96–98].

Increased the amount of HA in the composite material also leads to the appearance of an endothermic effect near 115 °C and a shifting of the endothermic effect corresponding to the Curie transition to lower temperatures, which indicates a disruption of the crystal structure of the electrically active β -phase of the VDF-TeFE copolymer.

Fig. 5 shows XRD diagrams of the samples. On the XRD diagram for the pure VDF-TeFE copolymer, an intense reflection is observed at near 19.4°, corresponding to crystallographic planes (110,200) of an electrically active β -phase [99]. On the XRD diagram for HA powder, there are a few intensive peaks: 26.0° (002), 31.9° (211), 32.3° (112), 33.1° (300), 34.2° (202), 39.9° (310), 46.8° (222) and 49.6° (213), as well as weak peaks: 21.8° (200), 23.0° (111), 28.2° (210), 35.6° (301), 39.3° (212), 42.1° (311), 43.9° (113), 45.6° (203), 50.7° (321), 51.4° (410) and 52.2° (402), which correspond to the structure of HA (Ca₁₀(PO₄)₆(OH)₂).

The increase of the HA amount in the composite material results in a decrease in the size of the crystals (l) in the β -phase of the plane (110,200) (Fig. 5, insert). A shift of the β -phase reflection to lower 2θ angles with an increase of HA indicates a decrease in the density of the crystal lattice packing in the direction of a and b axes [100]. The increase in the intensity of reflection at 18.9° (corresponding crystallographic plane (020) of the γ -phase) and the intensity of the halo at 18° (corresponds to the paraelectric α -phase) with a decrease in the intensity of the reflection at 19.4° indicates the increase of a γ electrically active phase and a paraelectric α -phase with an increasing proportion of HA in the composite material. Thus, XRD studies confirm the difficulty of crystallization of the copolymer VDF-TeFE as the electrically active β -phase in the presence of HA, which is similar to the conclusion of DSC studies.

Infrared spectra of the samples are shown in Fig. 6. There are several absorption bands characteristic of conformations of macromolecules with electrically active properties at 840 cm⁻¹, 880 cm⁻¹, 1328 cm⁻¹ (TTT - chain conformation) and 822 cm⁻¹ (T_3GT_3G - chain conformation) for the coating of the pure copolymer VDF-TeFE [67,101]. Additionally, present in the spectrum are bands at 617 cm⁻¹ and 925 cm⁻¹, characteristic of $TGTG$ - chain conformation with paraelectric

properties [67,102]. Thus, the polymer chains are present in the initial polymer film in all three conformational phases, but the presence of a strong absorption band at 840 cm⁻¹, characteristic for molecule fragments with long *trans* sequences, leads to the conclusion that the preferred conformation of the polymer molecules in the film is the most electrically active (TTT) chain conformation.

The increase in HA amount in the composite material results in the appearance of absorption bands in the spectrum at 560 cm⁻¹, 600 cm⁻¹ ($\nu_4PO_4^{3-}$), 630 cm⁻¹ (vibration mode OH⁻), the wide shoulder at 1024 cm⁻¹ (PO_4^{3-}), and bands at 1090 cm⁻¹ ($\nu_3PO_4^{3-}$) and 963 cm⁻¹ ($\nu_1PO_4^{3-}$) [103,104]. The presence of characteristic absorption bands at 840 cm⁻¹, 880 cm⁻¹, 1328 cm⁻¹, 822 cm⁻¹, 617 cm⁻¹ and 925 cm⁻¹ indicates the presence in the composite copolymer VDF-TeFE macromolecules of all three polymorphic conformations. The absence of new absorption bands, as well as the absence of shifts of characteristic absorption bands at 1058 cm⁻¹, 1156 cm⁻¹, 1395 cm⁻¹ and 1430 cm⁻¹, characteristic of the VDF-TeFE copolymer, suggests the absence of significant changes in the chemical copolymer structure during the formation of the composite material.

3.1. In vitro biology study

Table 3 presents the study of cytotoxicity of the samples using flow cytometry, indicating high levels of biocompatibility.

The cytotoxicity results (Table 3) revealed no significant differences in the number of viable cells and of necrotic and apoptotic cells cultured on coatings of the pure copolymer VDF-TeFE and on composite coatings with different amounts of HA. Thus, the research confirms the absence of cytotoxicity for the VDF-TeFE copolymer of and the composites with different HAP amounts.

Fig. 7 presents images of DAPI labeled cells on the surface of the coatings. The film of the pure copolymer VDF-TeFE has a low cell adhesion ability (Fig. 7a, Table 4), because it has a low roughness and a low surface energy, impeding cell attachment [91]. Low levels of cell adhesion to unpolarized PVDF samples were previously observed [59].

The increase of the HA amount of the composite material to 50% increases the number of adhered cells by >5 times (Fig. 7b, Table 4) compared with the control sample. This is associated with an increase in the hydrophilicity and surface roughness of the composite coating. Noteworthy is the fact that the formation of cell agglomerates on the surface of the composite material containing 50% of copolymer of VDF-TeFE is probably due to the presence of areas where HA particles extrude from the surface of the composite material; thus creating better conditions for cell attachment compared to the rest of the surface. Reduction of the VDF-TeFE copolymer to 35 or 25% does not lead to a significant increase in the number of cells adhered to the surface (Table 4). However, reducing the VDF-TeFE copolymer amount leads to changes in the adhesive structure of the cells on the surface of the composite materials (Fig. 7 c–d). Cells preferentially adhere around the pores of the composite material, not penetrating into them, probably because of poor liquid penetration into the internal pore space of the coatings.

Table 5
Effect of the tested samples on the geometric and histological characteristics of tissues growing subcutaneously from the bone marrow during the ectopic osteogenesis assay, $X \pm SD$ (S.E.M).

The samples studied, $n = 4$ in each group	Bone marrow (initial levels before implantation)	Tissue lamellae properties (after implantation)	
	Area, mm ²	Area, % of initial level	Histological composition
100% VDF-TeFE	6.9 ± 1.0 (0.5)	133 ± 109 (54)	Connective (Fig. 8, Panel a) and adipose (Panel b) tissues
50% VDF-TeFE	6.2 ± 1.2 (0.6)	206 ± 142 (71)	Bone with marrow (Fig. 8, Panel c) in 3 cases; connective tissue in 1 case (Panel d)
35% VDF-TeFE	4.8 ± 1.6 (0.8)	162 ± 124 (62)	Bone tissue with bone marrow (Fig. 8e,f)
25% VDF-TeFE	6.1 ± 1.5 (0.8)	123 ± 102 (51)	Bone with marrow (Fig. 8, Panel g) in 3 cases; thin bone lamella with connective tissue in 1 case (Panel h)

4 = the number of samples tested; statistical differences ($P < 0.05$) between all groups were not significant according to Mann–Whitney's U test.

Thus, as expected, an increase in the HA amount in the composite material is a key factor which leads to increased adhesion properties of the composite material for multipotent stem cells.

Because remodeling of bone occurs through the activation of osteoblasts located in the zone of damage, as well as through attraction of mesenchymal cells and their subsequent differentiation into osteoblasts, the anatomical location, fixing type, state of the implant bed

and surrounding tissue, and biological properties of the latter all have a major impact on the processes of osteoconduction [105]. Specifically, having a good blood supply to the fracture site providing inflow of mesenchymal cells is key to the formation of high-grade bone [106,107].

The disk samples coated with bone marrow and implanted subcutaneously, meet the requirements of having a significant number of

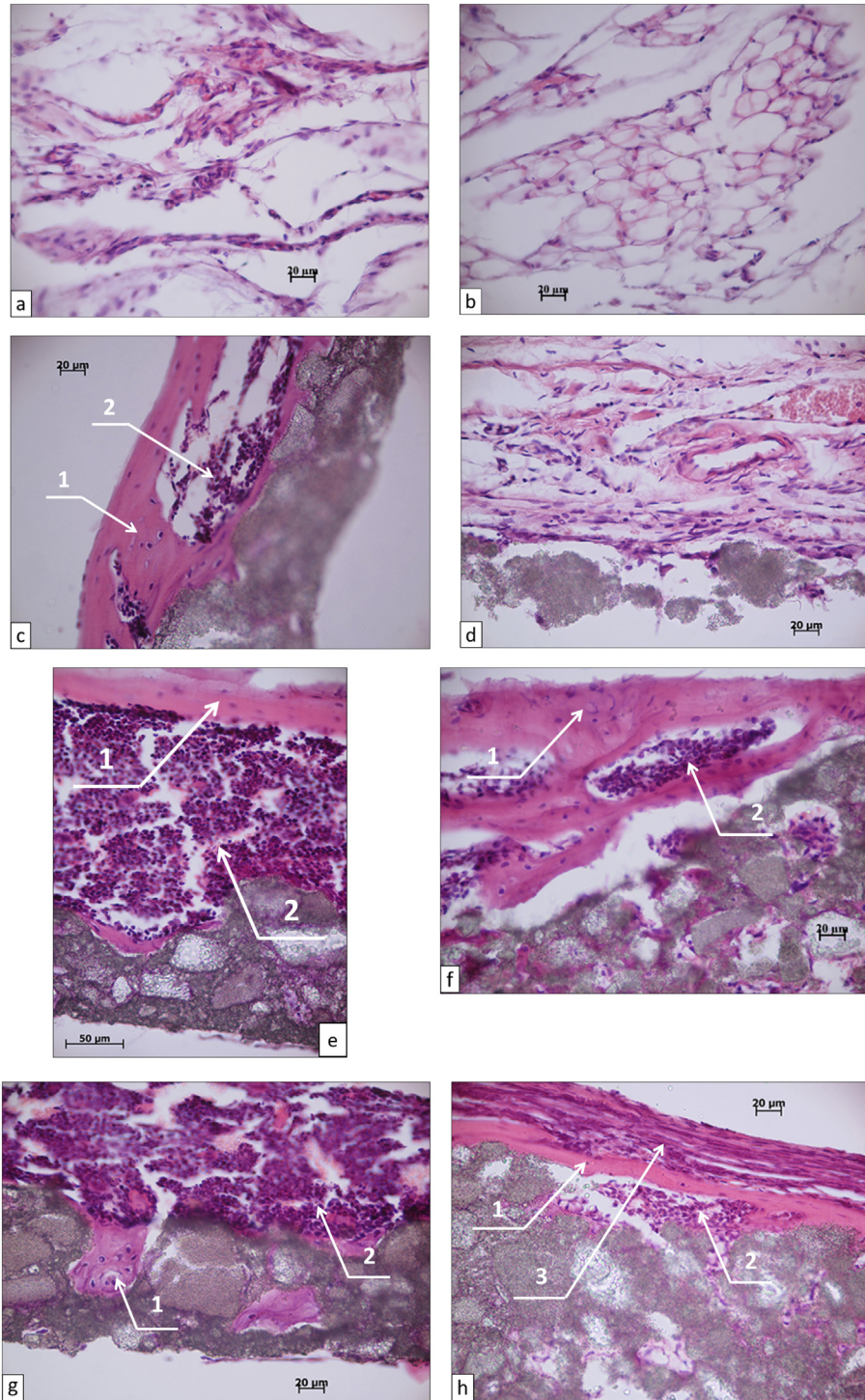


Fig. 8. Histological sections of tissue lamellae, grown on pure VDF-TeFE (a and b), 50% VDF-TeFE (c and d), VDF-TeFE 35% (e and f), 25% VDF-TeFE (g and h) in mouse subcutaneous test. Connective (a,d) and adipose (b) tissues only, bone tissue with bone marrow cells (c, e–g) and fibrous connective tissue (h) are shown. Hematoxylin – eosin staining. Arrows marked 1, 2 and 3 point to bone, marrow and fibrous connective tissue in lamella composition respectively.

Table 6
Pull-off force for various FINs.

Type of FIN	Pull-off force, N <i>n</i> = 4	Separation tension, MPa
Steel FIN without coating	140 ± 20	356 ± 10
Titanium FIN coated using MAO technology	258 ± 36	529 ± 30
Steel FIN with the composite coating	230 ± 23	557 ± 10

adipose-derived mesenchymal cells and a good blood supply. Therefore, the test of ectopic bone formation simulates the conditions of FIN in the medullary canal well.

Visual inspection of the site of implantation surrounding the disks with the test coatings showed no signs of inflammation, hypersensitivity or tissue sensation in all groups. Implants were surrounded by a thin

stromal capsule, which had a slight grip to the surface of the samples and could be easily removed. Tissue lamellae were universal for the samples (16 out of 16 samples) with the tissue area increasing to 123–206% of the corresponding initial values of bone marrow area (Table 5). This increase suggests the benefit of the coatings on promoting adhesion and bone marrow proliferation on the surface of implants.

Histological analysis of the tissue lamellae grown on the surface of the pure copolymer VDF-TeFE demonstrated connective (Table 5, Fig. 8a) and adipose (Table 5, Fig. 8b) tissues only. Whereas on the surface of composite coatings a formation of bone tissue with bone marrow (Table 5, Fig. 8c, e–g) and connective tissue (Fig. 8h) was observed in 11 out of 12 cases (92%) of composites. Therefore it can be concluded that tested samples promote adhesion and cell proliferation on the surface of implants under constant biomechanical cyclic loads caused by movement of muscles and the skin of laboratory animals. Since the initial values of bone marrow area did not differ statistically, the area of the

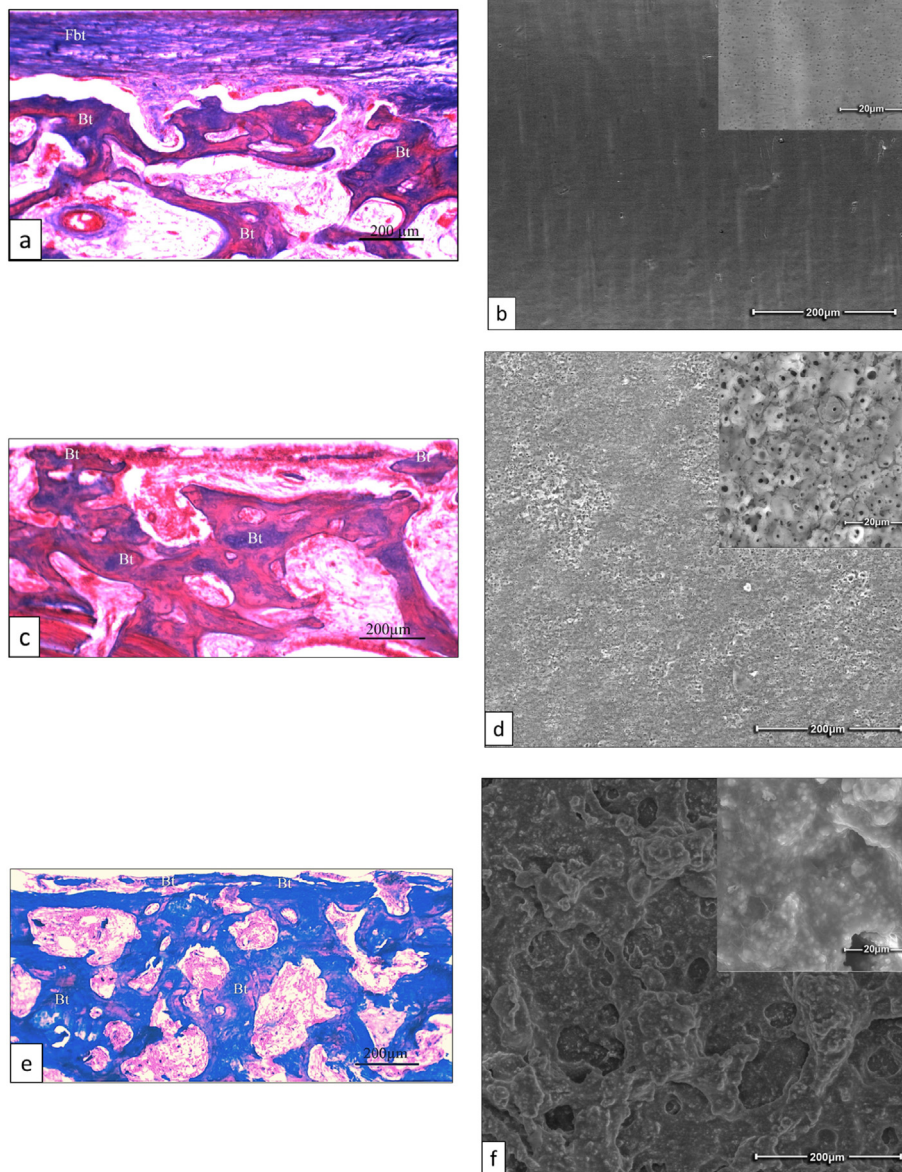


Fig. 9. Formation of a bone tissue envelope around the FIN and its dependence on the surface architecture. Light microscopy of histostructural bone envelope organization for stainless steel Kirschner wires (a), titanium wire with CaP coating produced with MAO technology (c), stainless steel wire with a composite coating (e), where Fbt and Bt indicate fibrous tissue and trabecular bone respectively. Scanning electron microscopy of the surface architecture for stainless steel Kirschner wires (b), titanium wire with CaP coating produced with MAO technology (d) and stainless steel wire with a composite coating (f).

tissue lamellae and the type of the tissue formed on the surface of the implants was caused by the physicochemical characteristics of the coatings.

It is known that the histological conduction is an important but not sufficient condition for the ectopic bone formation. The decisive role in the process of bone formation plays physical and chemical properties of the implant, such as the presence of CaP and the topology of the surface of the implant [108–111].

Nevertheless, no statistical increase in the area of tissue lamellae was detected for the groups tested (Table 5). Probably, the roughness and CaP amounts in the pure copolymer VDF-TeFE and its composites have no critical role for cell adhesion and tissue conduction process. Vice versa, the lack of these physical and chemical features hinders the differentiation of cells into osteogenic direction that was estimated by histological composition (Table 5).

Indeed, composite coatings containing 50% VDF-TeFE in 75% of cases (3 out of 4) were characterized by bone and bone marrow growth on the surface of samples (Table 5, Fig. 8c). One tissue lamella with vascularized loose irregular connective tissue on the surface of the sample can be classified as a failure of implantation (Table 5, Fig. 8d).

Tissue lamellae on the surface of coatings containing 35% VDF-TeFE were formed of bone and bone marrow (Table 5, Fig. 8e, f). Tissue lamellae on the surface of coatings containing 25% VDF-TeFE showed growth of bone tissue into the porous structure of the composite material (Fig. 8g). Some thin bone lamellae with weak bone marrow were covered with thick layers (20–40 μm) of fibrous connective tissue (Fig. 8h). The development of a bone through cartilage stage (endochondral ossification) is required for remodeling of hematopoietic tissue from the hematopoietic stem cells. Another way is the formation of bone without bone marrow by stromal stem cells, bypassing the stage of cartilage, by ossification of connective tissue [112]. Probably, it assumes bone formation in 25% cases (Table 5) on 25% VDF-TeFE coatings by means of ossification of connective tissue mainly.

Our research has shown that composite coatings containing 35% VDF-TeFE probably are optimal due to the combination of beneficial physico-chemical and biological properties. In particular, they have high flexibility, sufficient adhesive strength to nailing in the spongy bone tissue and possess rough surface topography providing a high biological activity. At the same time the polymeric binder is in crystalline phases with ferroelectric properties which promote the high biological activity of these composite coatings on the surface of the metal FIN. Given the constant influence of mechanical stresses from the bone and surrounding muscle it can be expected that the composite coating containing 35% VDF-TeFE will contribute to osteoinductive and osteoconductive processes not only due to the active filler, but also due to its ferroelectric properties.

One of the common ways to assess osteoinductive and osteoconductive properties of implants for orthopedics and traumatology is a test developed by Nakamura [113,114]. The test relates the value of the effort necessary for the separation of the implant from bio active surface of the bone bed with its osteoinductive and osteoconductive capacity. Results of bond strength studies of various FINs with bone tissue are presented in Table 6.

Studies demonstrated that the steel FIN with a smooth surface has the smallest pull-off force (Table 6). Microporous CaP layer formed on the surface of the titanium FIN produced > 130% increase in the value of pull-off force compared to the uncoated FIN. Steel implants with the bioactive composite ferroelectric coating with 35% VDF-TeFE copolymer amount demonstrated adhesion to the bone tissue comparable to that for titanium FIN coated using MAO technology. The significant difference in bond strength indicates high osteoinductive properties of the composite coating formed on the steel FIN which is confirmed by histological examination of the tissue around the FIN.

Fibrous tissue layer is formed to a thickness up to 2 mm around the uncoated steel FIN, which isolates the surface of FIN. The formation of bone envelope occurs on the periphery of the fibrous ring and

is characterized by depleted trabecular network. Thus, the use of the uncoated steel FIN is histologically characterized by distant osteogenesis (Fig. 9a). Because the anatomical placement of all FINs is characterized by optimal conditions of circulation and a high level of mesenchymal cells capable of differentiating into osteoblasts, the low osteoinductive properties of the uncoated steel FIN are due to the lack of surface conditions necessary for the attachment and proliferation of mesenchymal cells. These conditions are low roughness, the lack of CaP, and possible diffusion of the implant corrosion products into the surrounding tissue.

The titanium FIN coated with CaP using MAO technology is characterized by the absence of the fibrous tissue ring around the FIN. Young bone of trabecular structure was formed around titanium FIN which is fused with the endosteal surface of the medullary canal (Fig. 9b). Formation of the bone tissue of dense trabecular structure indicates high osteoinductive properties of CaP coatings obtained by MAO technology, which confirm the earlier literature results [14]. High osteoinductive properties of these coatings are due to the microporous structure relief reminiscent of the structure of the young bone, which facilitates the adhesion of mesenchymal cells. Typically, CaP coatings produced by MAO technology contain a significant amount of readily soluble calcium phosphates that induces the differentiation of mesenchymal cells into osteoblasts, and the absence of toxic corrosion products is a powerful factor stimulating osteogenesis process.

The histological picture around a stainless steel FIN with a composite coating that contains 35% VDF-TeFE (Fig. 9c) is comparable to the histological picture around the titanium FIN with CaP coating manufactured by MAO technology. Bone tissue of a dense trabecular structure adheres to the surface of the FIN without a fibrous tissue layer. Formation of the bone tissue of a dense trabecular structure indicates high osteoinductive properties of the coating.

Undoubtedly, high osteoinductive properties of FINs with composite coating, as is the case with the titanium FIN, are largely due to the rough surface of the coating. On the other hand VDF-TeFE copolymer film acts as a “primer” layer forming the coating that protects the metal in FIN from corrosion and blocks the exit of potentially toxic products into the surrounding tissue. However, it should be noted that on the surface of the composite coating the amount of calcium and phosphorus ions, needed for osteogenic differentiation, is less as, firstly, the biologically active filler in this case is highly crystalline HAP whose solubility in physiological media is significantly lower than the amorphous calcium phosphate on the surface of the titanium FIN, and, secondly, the concentration of the ions is less because the coating material is a composite.

Given the anatomical location of the implant and the continuous mechanical loading on FINs it is hypothesized that high osteoinductive properties of the composite material are largely due to the piezoelectric properties of the polymeric binder, a significant part of which is crystallized in the electrically active β - and γ -phases even for high amount of HA in the composite. Most likely mechanical stresses acting on the FIN cause continuous changes in its surface potential which is a powerful factor in promoting osteoinduction. This fact is confirmed by literature where the in vitro system demonstrated better adhesion of osteoblasts to the surface of PVDF film under mechanical stimulation [115]. Other research determined the optimal proportion of the electrically active β -phase as well as the osteogenic differentiation of MMSC in the presence of ferroelectric non-woven materials, even in the absence of calcium phosphate [57].

It should be noted that a further significant increase in clinical potential of FINs with composite coating is possible by using fast dissolving biologically active calcium phosphates as filler, such as amorphous calcium phosphate, tricalcium phosphate, carbonate-substituted hydroxyapatite, etc. Probably substantial reserves of increasing clinical potential of piezoelectric biologically active composites are in optimizing electrical properties of the piezoelectric binder in particular the use of additional “positive” or “negative” polarization during the formation of the composite material and further optimization of the crystal

structure by optimizing the process parameters such as heating and cooling modes. A significant potential to increase biological activity is also in the modification of the surface of a composite material to increase the surface hydrophilicity [116–118], which will improve the adhesion properties to the surface of cells and tissues.

4. Conclusion

The paper demonstrated the possibility of creating osteoinductive composite materials for use as a coating for flexible intramedullary nails. The effect of the amount of VDF-TeFE on the structure and properties of osteoinductive composites was investigated. It was shown that a decrease in the amount of VDF-TeFE in the coating increased the porosity of the composite material, but reduced the cohesive strength and elasticity of the coating. Increasing the HA amount in the composite material resulted in VDF-TeFE copolymer crystallization into predominantly β and γ electroactive phases. An ectopic bone formation assay demonstrated that the composite materials are non-toxic and have the ability to produce bone. The stimulatory effect of the coatings for the formation of young bone in a trabecular structure, which fills the volume of medullary canal, was established. The effect allows an increase in the total volume of bone tissue, and as a result, an elevation of the strength of cortical bones. The prospects of the use of the osteoinductive coatings in the ESIF technique were demonstrated.

Acknowledgments

This research was funded by Russian Science Foundation (project No 16-13-10239) and performed in Tomsk Polytechnic University.

References

- [1] J.N. Ligier, J.P. Metaizeau, J. Prévot, P. Lascombes, Elastic stable intramedullary nailing of femoral shaft fractures in children, *J. Bone Joint Surg. Br.* 70 (1988) 74–77 <http://www.ncbi.nlm.nih.gov/pubmed/3339064>.
- [2] D. Popkov, A. Popkov, T. Haumont, P. Journeau, P. Lascombes, Flexible intramedullary nail use in limb lengthening, *J. Pediatr. Orthop.* 30 (2010) 910–918, <http://dx.doi.org/10.1097/BPO.0b013e3181f0eaf9>.
- [3] D. Popkov, P. Lascombes, A. Popkov, P. Journeau, T. Haumont, Role of the flexible intramedullary nailing in limb lengthening in children: comparative study based on the series of 294 lengthenings, *Eur. Orthop. Traumatol.* 3 (2012) 17–24, <http://dx.doi.org/10.1007/s12570-012-0090-1>.
- [4] G.A. Ilizarov, Basic principles of transosseous compression and distraction osteosynthesis, *Ortop. Travmatol. Protez.* 32 (1971) 7–15.
- [5] D. Popkov, P. Journeau, A. Popkov, T. Haumont, P. Lascombes, Ollier's disease limb lengthening: should intramedullary nailing be combined with circular external fixation? *Orthop. Traumatol. Surg. Res.* 96 (2010) 348–353, <http://dx.doi.org/10.1016/j.otsr.2010.01.002>.
- [6] T. Jager, D. Popkov, P. Lascombes, A. Popkov, P. Journeau, Elastic intramedullary nailing as a complement to Ilizarov's method for forearm lengthening: a comparative pediatric prospective study, *Orthop. Traumatol. Surg. Res.* 98 (2012) 376–382, <http://dx.doi.org/10.1016/j.otsr.2012.01.007>.
- [7] A. Aranovich, A. Popkov, D. Barbier, D. Popkov, Femoral lengthening by combined technique in melorheostosis: a case report, *Eur. Orthop. Traumatol.* 5 (2014) 175–179, <http://dx.doi.org/10.1007/s12570-013-0220-4>.
- [8] S.V. Dorozhkin, Calcium orthophosphate deposits: preparation, properties and biomedical applications, *Mater. Sci. Eng. C* 55 (2015) 272–326, <http://dx.doi.org/10.1016/j.msec.2015.05.033>.
- [9] R.Z. LeGeros, Calcium phosphate-based osteoinductive materials, *Chem. Rev.* 108 (2008) 4742–4753, <http://dx.doi.org/10.1021/cr800427g>.
- [10] I.M. Ir'ianov, N.A. Kir'ianov, A.V. Popkov, Fracture healing under intramedullary insertion of wires with hydroxyapatite coating, *Vestn. Ross. Akad. Med. Nauk* (2014) 127–132 <http://www.ncbi.nlm.nih.gov/pubmed/25563014>.
- [11] A.V. Popkov, N.A. Kononovich, E.N. Gorbach, S.I. Tverdokhlebov, Y.M. Irianov, D.A. Popkov, Bone healing by using Ilizarov external fixation combined with flexible intramedullary nailing versus Ilizarov external fixation alone in the repair of tibial shaft fractures: experimental study, *Sci. World J.* 2014 (2014) 1–8, <http://dx.doi.org/10.1155/2014/239791>.
- [12] A. Popkov, A. Aranovich, D. Popkov, Results of deformity correction in children with X-linked hereditary hypophosphatemic rickets by external fixation or combined technique, *Int. Orthop.* 39 (2015) 2423–2431, <http://dx.doi.org/10.1007/s00264-015-2814-7>.
- [13] Y. Li, I.-S. Lee, F.-Z. Cui, S.-H. Choi, The biocompatibility of nanostructured calcium phosphate coated on micro-arc oxidized titanium, *Biomaterials* 29 (2008) 2025–2032, <http://dx.doi.org/10.1016/j.biomaterials.2008.01.009>.
- [14] Y. Wang, H. Yu, C. Chen, Z. Zhao, Review of the biocompatibility of micro-arc oxidation coated titanium alloys, *Mater. Des.* 85 (2015) 640–652, <http://dx.doi.org/10.1016/j.matdes.2015.07.086>.
- [15] N. Goyal, A.N. Aggarwal, P. Mishra, A. Jain, Randomized controlled trial comparing stabilization of fresh close femoral shaft fractures in children with titanium elastic nail system versus stainless steel elastic nail system, *Acta Orthop. Belg.* 80 (2014) 69–75 (accessed October 13, 2015) <http://www.ncbi.nlm.nih.gov/pubmed/24873088>.
- [16] E.J. Wall, Complications of titanium and stainless steel elastic nail fixation of pediatric femoral fractures, *J. Bone Jt. Surg.* 90 (2008) 1305, <http://dx.doi.org/10.2106/JBJS.G.00328>.
- [17] U.S. Mani, C.T. Sabatino, S. Sabharwal, D.J. Svach, A. Suslak, F.F. Behrens, Biomechanical comparison of flexible stainless steel and titanium nails with external fixation using a femur fracture model, *J. Pediatr. Orthop.* 26 (2006) 182–187, <http://dx.doi.org/10.1097/01.bpo.0000218525.28739.7e>.
- [18] S. Weiner, H.D. Wagner, The material bone: structure–mechanical function relations, *Annu. Rev. Mater. Sci.* 28 (1998) 271–298, <http://dx.doi.org/10.1146/annurev.matsci.28.1.271>.
- [19] G.W. Hastings, F.A. Mahmud, Electrical effects in bone, *J. Biomed. Eng.* 10 (1988) 515–521, [http://dx.doi.org/10.1016/0141-5425\(88\)90109-4](http://dx.doi.org/10.1016/0141-5425(88)90109-4).
- [20] E. Fukada, I. Yasuda, On the piezoelectric effect of bone, *J. Phys. Soc. Jpn.* 12 (1957) 1158–1162, <http://dx.doi.org/10.1143/JPSJ.12.1158>.
- [21] C. Halperin, S. Mutchnik, A. Agronin, M. Molotskii, P. Urenski, M. Salai, G. Rosenman, Piezoelectric effect in human bones studied in nanometer scale, *Nano Lett.* 4 (2004) 1253–1256, <http://dx.doi.org/10.1021/nl049453i>.
- [22] M.A. El Messierly, G.W. Hastings, S. Rakowski, Ferro-electricity of dry cortical bone, *J. Biomed. Eng.* 1 (1979) 63–65, [http://dx.doi.org/10.1016/0141-5425\(79\)90013-X](http://dx.doi.org/10.1016/0141-5425(79)90013-X).
- [23] S.R. Pollack, N. Petrov, R. Salzman, G. Brankov, R. Blagoeva, An anatomical model for streaming potentials in osteons, *J. Biomech.* 17 (1984) 627–636, [http://dx.doi.org/10.1016/0021-9290\(84\)90094-0](http://dx.doi.org/10.1016/0021-9290(84)90094-0).
- [24] R.C. Riddle, H.J. Donahue, From streaming-potentials to shear stress: 25 years of bone cell mechanotransduction, *J. Orthop. Res.* 27 (2009) 143–149, <http://dx.doi.org/10.1002/jor.20723>.
- [25] S. Wu, X. Liu, K.W.K. Yeung, C. Liu, X. Yang, Biomimetic porous scaffolds for bone tissue engineering, *Mater. Sci. Eng. R. Rep.* 80 (2014) 1–36, <http://dx.doi.org/10.1016/j.mser.2014.04.001>.
- [26] F. Barrère, T.A. Mahmood, K. de Groot, C.A. van Blitterswijk, Advanced biomaterials for skeletal tissue regeneration: instructive and smart functions, *Mater. Sci. Eng. R. Rep.* 59 (2008) 38–71, <http://dx.doi.org/10.1016/j.mser.2007.12.001>.
- [27] D.M. Ciombor, R.K. Aaron, The role of electrical stimulation in bone repair, *Foot Ankle Clin.* 10 (2005) 579–593, <http://dx.doi.org/10.1016/j.fcl.2005.06.006>.
- [28] M.E. Mycielska, M.B.A. Djamgoz, Cellular mechanisms of direct-current electric field effects: galvanotaxis and metastatic disease, *J. Cell Sci.* 117 (2004) 1631–1639, <http://dx.doi.org/10.1242/jcs.01125>.
- [29] K. Yamashita, N. Oikawa, T. Umegaki, Acceleration and deceleration of bone-like crystal growth on ceramic hydroxyapatite by electric poling, *Chem. Mater.* 8 (1996) 2697–2700, <http://dx.doi.org/10.1021/cm9602858>.
- [30] A. Kotwal, Electrical stimulation alters protein adsorption and nerve cell interactions with electrically conducting biomaterials, *Biomaterials* 22 (2001) 1055–1064, [http://dx.doi.org/10.1016/S0142-9612\(00\)00344-6](http://dx.doi.org/10.1016/S0142-9612(00)00344-6).
- [31] C.A.L. Bassett, Biologic significance of piezoelectricity, *Calcif. Tissue Res.* 1 (1967) 252–272, <http://dx.doi.org/10.1007/BF02008098>.
- [32] C.A. BASSETT, R.J. PAWLJUK, R.O. BECKER, Effects of electric currents on bone in vivo, *Nature* 204 (1964) 652–654, <http://dx.doi.org/10.1038/204652a0>.
- [33] A. Marino, J. Barsotti, G. de Vito, C. Filippeschi, B. Mazzolai, V. Piazza, M. Labardi, V. Mattoli, G. Ciofani, Two-photon lithography of 3D nanocomposite piezoelectric scaffolds for cell stimulation, *ACS Appl. Mater. Interfaces* 7 (2015) 25574–25579, <http://dx.doi.org/10.1021/acsami.5b08764>.
- [34] G. Ciofani, L. Ricotti, C. Canale, D. D'Alessandro, S. Berrettini, B. Mazzolai, V. Mattoli, Effects of barium titanate nanoparticles on proliferation and differentiation of rat mesenchymal stem cells, *Colloids Surf. B Biointerfaces* 102 (2013) 312–320, <http://dx.doi.org/10.1016/j.colsurfb.2012.08.001>.
- [35] J.P. Ball, B.A. Mound, J.C. Nino, J.B. Allen, Biocompatible evaluation of barium titanate foamed ceramic structures for orthopedic applications, *J. Biomed. Mater. Res. A* 102 (2014) 2089–2095, <http://dx.doi.org/10.1002/jbma.34879>.
- [36] J.B. Park, B.J. Kelly, G.H. Kenner, A.F. von Recum, M.F. Grether, W.W. Coffeen, Piezoelectric ceramic implants: in vivo results, *J. Biomed. Mater. Res.* 15 (1981) 103–110, <http://dx.doi.org/10.1002/jbm.820150114>.
- [37] B. Liu, L. Chen, C. Shao, F. Zhang, K. Zhou, J. Cao, D. Zhang, Improved osteoblasts growth on osteomimetic hydroxyapatite/BaTiO₃ composites with aligned lamellar porous structure, *Mater. Sci. Eng. C* 61 (2016) 8–14, <http://dx.doi.org/10.1016/j.msec.2015.12.009>.
- [38] F. Jianqing, Y. Huipin, Z. Xingdong, Promotion of osteogenesis by a piezoelectric biological ceramic, *Biomaterials* 18 (1997) 1531–1534, [http://dx.doi.org/10.1016/S0142-9612\(97\)80004-X](http://dx.doi.org/10.1016/S0142-9612(97)80004-X).
- [39] Y. Zhang, L. Chen, J. Zeng, K. Zhou, D. Zhang, Aligned porous barium titanate/hydroxyapatite composites with high piezoelectric coefficients for bone tissue engineering, *Mater. Sci. Eng. C* 39 (2014) 143–149, <http://dx.doi.org/10.1016/j.msec.2014.02.022>.
- [40] A.V. Zanfir, G. Voicu, C. Busuioac, S.I. Jinga, M.G. Albu, F. Iordache, New Coll-HA/BT composite materials for hard tissue engineering, *Mater. Sci. Eng. C* 62 (2016) 795–805, <http://dx.doi.org/10.1016/j.msec.2016.02.041>.
- [41] S. Ke, Y. Yang, L. Ren, Y. Wang, Y. Li, H. Huang, Dielectric behaviors of PHBHHx-BaTiO₃ multifunctional composite films, *Compos. Sci. Technol.* 72 (2012) 370–375, <http://dx.doi.org/10.1016/j.compscitech.2011.11.028>.
- [42] M. Airimioaei, R. Stanculescu, V. Preuntu, C. Ciomaga, N. Horchidan, S. Tascu, D. Lutic, A. Pui, L. Mitoseriu, Effect of particle size and volume fraction of BaTiO₃ powders on the functional properties of BaTiO₃/poly(ϵ -caprolactone) composites, *Mater.*

- Chem. Phys. 182 (2016) 246–255, <http://dx.doi.org/10.1016/j.matchemphys.2016.07.029>.
- [43] X. Zhang, C. Zhang, Y. Lin, P. Hu, Y. Shen, K. Wang, S. Meng, Y. Chai, X. Dai, X. Liu, Y. Liu, X. Mo, C. Cao, S. Li, X. Deng, L. Chen, Nanocomposite membranes enhance bone regeneration through restoring physiological electric microenvironment, *ACS Nano* 10 (2016) 7279–7286, <http://dx.doi.org/10.1021/acsnano.6b02247>.
- [44] H.B. Lopes, T. de S. Santos, F.S. de Oliveira, G.P. Freitas, A.L. de Almeida, R. Gimenes, A.L. Rosa, M.M. Beloti, Poly(vinylidene-trifluoroethylene)/barium titanate composite for in vivo support of bone formation, *J. Biomater. Appl.* 29 (2013) 104–112, <http://dx.doi.org/10.1177/0885328213515735>.
- [45] H.B. Lopes, E.P. Ferraz, A.L.G. Almeida, P. Florio, R. Gimenes, A.L. Rosa, M.M. Beloti, Participation of MicroRNA-34a and RANKL on bone repair induced by poly(vinylidene-trifluoroethylene)/barium titanate membrane, *J. Biomater. Sci. Polym. Ed.* 27 (2016) 1369–1379, <http://dx.doi.org/10.1080/09205063.2016.1203217>.
- [46] P. Vaněk, Z. Kolská, T. Luxbacher, J.A.L. García, M. Lehocký, M. Vandrovcová, L. Bačáková, J. Petzelt, Electrical activity of ferroelectric biomaterials and its effects on the adhesion, growth and enzymatic activity of human osteoblast-like cells, *J. Phys. D. Appl. Phys.* 49 (2016) 175403, <http://dx.doi.org/10.1088/0022-3727/49/17/175403>.
- [47] N.C. Carville, L. Collins, M. Manzo, K. Gallo, B.I. Lukasz, K.K. McKayed, J.C. Simpson, B.J. Rodriguez, Biocompatibility of ferroelectric lithium niobate and the influence of polarization charge on osteoblast proliferation and function, *J. Biomed. Mater. Res. A* 103 (2015) 2540–2548, <http://dx.doi.org/10.1002/jbm.a.35390>.
- [48] A.K. Dubey, R. Kinoshita, K. Kakimoto, Piezoelectric sodium potassium niobate mediated improved polarization and in vitro bioactivity of hydroxyapatite, *RSC Adv.* 5 (2015) 19638–19646, <http://dx.doi.org/10.1039/C5RA00771B>.
- [49] A. Bagchi, S.R.K. Meka, B.N. Rao, K. Chatterjee, Perovskite ceramic nanoparticles in polymer composites for augmenting bone tissue regeneration, *Nanotechnology* 25 (2014) 485101, <http://dx.doi.org/10.1088/0957-4484/25/48/485101>.
- [50] D.H. Yoon, B.I. Lee, P. Badheka, X. Wang, Barium ion leaching from barium titanate powder in water, *J. Mater. Sci. Mater. Electron.* 14 (2003) 165–169, <http://dx.doi.org/10.1023/A:1022306024907>.
- [51] S.-W. Yu, S.-T. Kuo, W.-H. Tuan, Y.-Y. Tsai, S.-F. Wang, Cytotoxicity and degradation behavior of potassium sodium niobate piezoelectric ceramics, *Ceram. Int.* 38 (2012) 2845–2850, <http://dx.doi.org/10.1016/j.ceramint.2011.11.056>.
- [52] J.S. de C. Campos, A.A. Ribeiro, C.X. Cardoso, Preparation and characterization of PVDF/CaCO₃ composites, *Mater. Sci. Eng. B* 136 (2007) 123–128, <http://dx.doi.org/10.1016/j.mseb.2006.09.017>.
- [53] C. Ribeiro, V. Sencadas, D.M. Correia, S. Lanceros-Méndez, Piezoelectric polymers as biomaterials for tissue engineering applications, *Colloids Surf. B Biointerfaces* 136 (2015) 46–55, <http://dx.doi.org/10.1016/j.colsurfb.2015.08.043>.
- [54] A.H. Rajabi, M. Jaffe, T.L. Arinze, Piezoelectric materials for tissue regeneration: a review, *Acta Biomater.* 24 (2015) 12–23, <http://dx.doi.org/10.1016/j.actbio.2015.07.010>.
- [55] K.S. Ramadan, D. Sameoto, S. Evoy, A review of piezoelectric polymers as functional materials for electromechanical transducers, *Smart Mater. Struct.* 23 (2014) 33001, <http://dx.doi.org/10.1088/0964-1726/23/3/033001>.
- [56] C. Ribeiro, D.M. Correia, S. Ribeiro, V. Sencadas, G. Botelho, S. Lanceros-Méndez, Piezoelectric poly(vinylidene fluoride) microstructure and poling state in active tissue engineering, *Eng. Life Sci.* 15 (2015) 351–356, <http://dx.doi.org/10.1002/elsc.201400144>.
- [57] S.M. Damaraju, S. Wu, M. Jaffe, T.L. Arinze, Structural changes in PVDF fibers due to electrospinning and its effect on biological function, *Biomed. Mater.* 8 (2013) 45007, <http://dx.doi.org/10.1088/1748-6041/8/4/045007>.
- [58] J. Pärssinen, H. Hammarén, R. Rahikainen, V. Sencadas, C. Ribeiro, S. Vanhatupa, S. Miettinen, S. Lanceros-Méndez, V.P. Hytönen, Enhancement of adhesion and promotion of osteogenic differentiation of human adipose stem cells by poled electroactive poly(vinylidene fluoride), *J. Biomed. Mater. Res. A* (2014) <http://dx.doi.org/10.1002/jbm.a.35234>.
- [59] C. Ribeiro, J. Pärssinen, V. Sencadas, V. Correia, S. Miettinen, V.P. Hytönen, S. Lanceros-Méndez, Dynamic piezoelectric stimulation enhances osteogenic differentiation of human adipose stem cells, *J. Biomed. Mater. Res. A* (2014) <http://dx.doi.org/10.1002/jbm.a.35368>.
- [60] J.J. Ficat, G. Escourrou, M.J. Fauran, R. Durroux, P. Ficat, C. Lacabanne, F. Micheron, Osteogenesis induced by bimorph polyvinylidene fluoride films, *Ferroelectrics* 51 (2011) 121–128, <http://dx.doi.org/10.1080/00150198308009062>.
- [61] A.A. Marino, J. Rosson, E. Gonzalez, L. Jones, S. Rogers, E. Fukada, Quasi-static charge interactions in bone, *J. Electrostat.* 21 (1988) 347–360, [http://dx.doi.org/10.1016/0304-3886\(88\)90036-8](http://dx.doi.org/10.1016/0304-3886(88)90036-8).
- [62] T. Furukawa, Recent advances in ferroelectric polymers, *Ferroelectrics* 104 (1990) 229–240, <http://dx.doi.org/10.1080/00150199008223826>.
- [63] V.V. Kochervinskii, The structure and properties of block poly(vinylidene fluoride) and systems based on it, *Russ. Chem. Rev.* 65 (2007) 865–913, <http://dx.doi.org/10.1070/RC1996v065n10ABEH000328>.
- [64] T. Furukawa, Ferroelectric properties of vinylidene fluoride copolymers, *Phase Transit.* 18 (1989) 143–211, <http://dx.doi.org/10.1080/01411598908206863>.
- [65] J.B. Lando, W.W. Doll, The polymorphism of poly(vinylidene fluoride). I. The effect of head-to-head structure, *J. Macromol. Sci., Part B: Phys.* 2 (1968) 205–218, <http://dx.doi.org/10.1080/00222346808212449>.
- [66] A.J. Lovinger, G.E. Johnson, H.E. Bair, E.W. Anderson, Structural, dielectric, and thermal investigation of the Curie transition in a tetrafluoroethylene copolymer of vinylidene fluoride, *J. Appl. Phys.* 56 (1984) 2412, <http://dx.doi.org/10.1063/1.334303>.
- [67] K. Tashiro, H. Kaito, M. Kobayashi, Structural changes in ferroelectric phase transitions of vinylidene fluoride-tetrafluoroethylene copolymers: 1. Vinylidene fluoride content dependence of the transition behaviour, *Polymer (Guildf)* 33 (1992) 2915–2928, [http://dx.doi.org/10.1016/0032-3861\(92\)90077-A](http://dx.doi.org/10.1016/0032-3861(92)90077-A).
- [68] J.B. Lando, W.W. Doll, The polymorphism of poly(vinylidene fluoride). I. The effect of head-to-head structure, *J. Macromol. Sci. B* 2 (1968) 205–218, <http://dx.doi.org/10.1080/00222346808212449>.
- [69] V.V. Kochervinskii, D.A. Kiselev, M.D. Malinkovich, A.S. Pavlov, I.A. Malyskhina, Local piezoelectric response, structural and dynamic properties of ferroelectric copolymers of vinylidene fluoride-tetrafluoroethylene, *Colloid Polym. Sci.* (2014) <http://dx.doi.org/10.1007/s00396-014-3435-1>.
- [70] E.N. Bolbasov, K.S. Stankevich, E.A. Sudarev, V.M. Bouznik, V.L. Kudryavtseva, L.V. Antonova, V.G. Matveeva, Y.G. Anissimov, S.I. Tverdokhlebov, The investigation of the production method influence on the structure and properties of the ferroelectric nonwoven materials based on vinylidene fluoride – tetrafluoroethylene copolymer, *Mater. Chem. Phys.* 182 (2016) 338–346, <http://dx.doi.org/10.1016/j.matchemphys.2016.07.041>.
- [71] E.N. Bolbasov, Y.G. Anissimov, A.V. Pustovoytov, I.A. Khlusov, A.A. Zaitsev, K.V. Zaitsev, I.N. Lapin, S.I. Tverdokhlebov, Ferroelectric polymer scaffolds based on a copolymer of tetrafluoroethylene with vinylidene fluoride: fabrication and properties, *Mater. Sci. Eng., C* 40 (2014) 32–41, <http://dx.doi.org/10.1016/j.msec.2014.03.038>.
- [72] E.N. Bolbasov, S.I. Tverdokhlebov, V.M. Busnik, A.V. Pustovoytov, Structure and properties of nonwoven materials based on copolymer of tetrafluoroethylene and vinylidene fluoride produced by aerodynamic formation, *Inorg. Mater. Appl. Res.* 6 (2015) 22–31, <http://dx.doi.org/10.1134/S2075113315010037>.
- [73] Z. Cui, E. Drioli, Y.M. Lee, Recent progress in fluoropolymers for membranes, *Prog. Polym. Sci.* 39 (2014) 164–198, <http://dx.doi.org/10.1016/j.progpolymsci.2013.07.008>.
- [74] L.-H. He, O.C. Standard, T.T.Y. Huang, B.A. Latella, M.V. Swain, Mechanical behaviour of porous hydroxyapatite, *Acta Biomater.* 4 (2008) 577–586, <http://dx.doi.org/10.1016/j.actbio.2007.11.002>.
- [75] V.M. Rogozhin, I.V. Akimova, Y.V. Smirnov, Determination of the porosity of spray-deposited coatings by hydrostatic weighing, *Sov. Powder Metall. Met. Ceram.* 19 (1980) 617–620, <http://dx.doi.org/10.1007/BF00790552>.
- [76] V.V. Kochervinskii, Specifics of structural transformations in poly(vinylidene fluoride)-based ferroelectric polymers in high electric fields, *Polym. Sci. Ser. C* 50 (2008) 93–121, <http://dx.doi.org/10.1134/S1811238208010062>.
- [77] J.C. Hicks, T.E. Jones, J.C. Logan, Ferroelectric properties of poly(vinylidene fluoride-tetrafluoroethylene), *J. Appl. Phys.* 49 (1978) 6092, <http://dx.doi.org/10.1063/1.324528>.
- [78] S. Tasaka, S. Miyata, Effects of crystal structure on piezoelectric and ferroelectric properties of copoly(vinylidene fluoride-tetrafluoroethylene), *J. Appl. Phys.* 57 (1985) 906, <http://dx.doi.org/10.1063/1.334691>.
- [79] A.J. Lovinger, Ferroelectric polymers, *Science* 80 (220) (1983) 1115–1121, <http://dx.doi.org/10.1017/CBO9781107415324.004>.
- [80] B. Ameduri, From vinylidene fluoride (VDF) to the applications of VDF-containing polymers and copolymers: recent developments and future trends, *Chem. Rev.* 109 (2009) 6632–6686, <http://dx.doi.org/10.1021/cr800187m>.
- [81] P. Martins, A.C. Lopes, S. Lanceros-Mendez, Electroactive phases of poly(vinylidene fluoride): determination, processing and applications, *Prog. Polym. Sci.* 39 (2014) 683–706, <http://dx.doi.org/10.1016/j.progpolymsci.2013.07.006>.
- [82] S.D. Vache, F. Oliveira, Y. Leterrier, V. Michaud, D. Damjanovic, J.-A.E. Manson, The effect of processing conditions on the morphology, thermomechanical, dielectric, and piezoelectric properties of P(VDF-TrFE)/BaTiO₃ composites, *J. Mater. Sci.* 47 (2012) 4763–4774, <http://dx.doi.org/10.1007/s10853-012-6362-x>.
- [83] R.I. Dmitrieva, I.R. Minullina, A.A. Bilibina, O.V. Tarasova, S.V. Anisimov, A.Y. Zaritsky, Bone marrow- and subcutaneous adipose tissue-derived mesenchymal stem cells: differences and similarities, *Cell Cycle* 11 (2012) 377–383, <http://dx.doi.org/10.4161/cc.11.2.18858>.
- [84] E.N. Bolbasov, I.N. Lapin, V.A. Svetlichnyi, Y.D. Lenivtseva, A. Malashicheva, Y. Malashichev, A.S. Golovkin, Y.G. Anissimov, S.I. Tverdokhlebov, The formation of calcium phosphate coatings by pulse laser deposition on the surface of polymeric ferroelectric, *Appl. Surf. Sci.* 349 (2015) 420–429, <http://dx.doi.org/10.1016/j.apsusc.2015.05.025>.
- [85] P. Kasten, J. Vogel, R. Luginbühl, P. Niemeyer, M. Tonak, H. Lorenz, L. Helbig, S. Weiss, J. Fellenberg, A. Leo, H.-G. Simank, W. Richter, Ectopic bone formation associated with mesenchymal stem cells in a resorbable calcium deficient hydroxyapatite carrier, *Biomaterials* 26 (2005) 5879–5889, <http://dx.doi.org/10.1016/j.biomaterials.2005.03.001>.
- [86] I.A. Khlusov, A.V. Karlov, Y.P. Sharkeev, V.F. Pichugin, Y.P. Kolobov, G.A. Shashkina, M.B. Ivanov, E.V. Legostaeva, G.T. Sukhikh, Osteogenic potential of mesenchymal stem cells from bone marrow in situ: role of physicochemical properties of artificial surfaces, *Bull. Exp. Biol. Med.* 140 (2005) 144–152, <http://dx.doi.org/10.1007/s10517-005-0431-y>.
- [87] H.W.C.G. Janet, R.W. Barbee, J.T. Bielitzki, L.A. Clayton, J.C. Donovan, C.F.M. Hendriksen, D.F. Kohn, N.S. Lipman, P.A. Locke, J. Melcher, F.W. Quimby, P.V. Turner, *G.A. Wood, Guide for the Care and Use of Laboratory Animals*, National Academies Press, Washington DC, 2011.
- [88] Y.H. An, K.L. Martin (Eds.), *Handbook of Histology Methods for Bone and Cartilage*, Humana Press, Totowa, NJ, 2003 <http://dx.doi.org/10.1007/978-1-59259-417-7>.
- [89] O.P. Terleeva, Y.P. Sharkeev, A.I. Slonova, I.V. Mironov, E.V. Legostaeva, I.A. Khlusov, E. Matykina, P. Skeldon, G.E. Thompson, Effect of microplasma modes and electrolyte composition on micro-arc oxidation coatings on titanium for medical applications, *Surf. Coat. Technol.* 205 (2010) 1723–1729, <http://dx.doi.org/10.1016/j.surfcoat.2010.10.019>.
- [90] K. El Hami, H. Yamada, K. Matsushige, Nanoscopic measurements of the electrostriction responses in P(VDF/TrFE) ultra-thin-film copolymer using atomic

- force microscopy, *Appl. Phys. A Mater. Sci. Process.* 72 (2001) 347–350, <http://dx.doi.org/10.1007/s003390000702>.
- [91] S.I. Tverdokhlebov, E.N. Bolbasov, E.V. Shesterikov, A.I. Malchikhina, V.A. Novikov, Y.G. Anissimov, Research of the surface properties of the thermoplastic copolymer of vinylidene fluoride and tetrafluoroethylene modified with radio-frequency magnetron sputtering for medical application, *Appl. Surf. Sci.* 263 (2012) 187–194, <http://dx.doi.org/10.1016/j.apsusc.2012.09.025>.
- [92] W. Li, Y. Zhu, D. Hua, P. Wang, X. Chen, J. Shen, Crystalline morphologies of P(VDF-TrFE) (70/30) copolymer films above melting point, *Appl. Surf. Sci.* 254 (2008) 7321–7325, <http://dx.doi.org/10.1016/j.apsusc.2008.05.339>.
- [93] D. Aronov, G. Rosenman, Trap state spectroscopy studies and wettability modification of hydroxyapatite nanobioceramics, *J. Appl. Phys.* 101 (2007) 34701, <http://dx.doi.org/10.1063/1.2433702>.
- [94] A.B.D. Cassie, S. Baxter, Wettability of porous surfaces, *Trans. Faraday Soc.* 40 (1944) 546, <http://dx.doi.org/10.1039/tf9444000546>.
- [95] Y. Murata, N. Koizumi, Ferroelectric behavior in vinylidene fluoride-tetrafluoroethylene copolymers, *Ferroelectrics* 92 (1989) 47–54, <http://dx.doi.org/10.1080/00150198908211305>.
- [96] A. Lonjon, P. Demont, E. Dantras, C. Lacabanne, Mechanical improvement of P(VDF-TrFE)/nickel nanowires conductive nanocomposites: influence of particles aspect ratio, *J. Non-Cryst. Solids* 358 (2012) 236–240, <http://dx.doi.org/10.1016/j.jnoncrysol.2011.09.019>.
- [97] J. Nunes-Pereira, A.C. Lopes, C.M. Costa, L.C. Rodrigues, M.M. Silva, S. Lanceros-Méndez, Microporous membranes of NaY zeolite/poly(vinylidene fluoride-trifluoroethylene) for Li-ion battery separators, *J. Electroanal. Chem.* 689 (2013) 223–232, <http://dx.doi.org/10.1016/j.jelechem.2012.10.030>.
- [98] A.S. Bhatt, D.K. Bhat, M.S. Santosh, Crystallinity, conductivity, and magnetic properties of PVDF-Fe₃O₄ composite films, *J. Appl. Polym. Sci.* 119 (2011) 968–972, <http://dx.doi.org/10.1002/app.32796>.
- [99] V. Kochervinskii, I. Malyshkina, A. Pavlov, N. Bessonova, A. Korlyukov, V. Volkov, N. Kozlova, N. Shmakova, Influence of parameters of molecular mobility on formation of structure in ferroelectric vinylidene fluoride copolymers, *J. Appl. Phys.* 117 (2015) 214101, <http://dx.doi.org/10.1063/1.4921851>.
- [100] A.J. Lovinger, D.D. Davis, R.E. Cais, J.M. Kometani, Compositional variation of the structure and solid-state transformations of vinylidene fluoride/tetrafluoroethylene copolymers, *Macromolecules* 21 (1988) 78–83, <http://dx.doi.org/10.1021/ma00179a017>.
- [101] K. Tashiro, H. Kaito, M. Kobayashi, Structural changes in ferroelectric phase transitions of vinylidene fluoride-tetrafluoroethylene copolymers: 2. Normal-modes analysis of the infra-red and Raman spectra at room temperature, *Polymer (Guildf)* 33 (1992) 2929–2933, [http://dx.doi.org/10.1016/0032-3861\(92\)90078-B](http://dx.doi.org/10.1016/0032-3861(92)90078-B).
- [102] Y.K.A. Low, N. Meenubharathi, N.D. Niphadkar, F.Y.C. Boey, K.W. Ng, α - and β -poly(vinylidene fluoride) evoke different cellular behaviours, *J. Biomater. Sci. Polym. Ed.* 22 (2011) 1651–1667, <http://dx.doi.org/10.1163/092050610X519471>.
- [103] A. Ślószarczyk, C. Paluszkiwicz, M. Gawlicki, Z. Paszkiewicz, The FTIR spectroscopy and QXRD studies of calcium phosphate based materials produced from the powder precursors with different ratios, *Ceram. Int.* 23 (1997) 297–304, [http://dx.doi.org/10.1016/S0272-8842\(96\)00016-8](http://dx.doi.org/10.1016/S0272-8842(96)00016-8).
- [104] A. Ślószarczyk, Z. Paszkiewicz, C. Paluszkiwicz, FTIR and XRD evaluation of carbonated hydroxyapatite powders synthesized by wet methods, *J. Mol. Struct.* 744–747 (2005) 657–661, <http://dx.doi.org/10.1016/j.molstruc.2004.11.078>.
- [105] D. Taylor, Bone maintenance and remodeling: a control system based on fatigue damage, *J. Orthop. Res.* 15 (1997) 601–606, <http://dx.doi.org/10.1002/jor.1100150417>.
- [106] E.A. Bayer, R. Gottardi, M.V. Fedorchak, S.R. Little, The scope and sequence of growth factor delivery for vascularized bone tissue regeneration, *J. Control. Release* 219 (2015) 129–140, <http://dx.doi.org/10.1016/j.jconrel.2015.08.004>.
- [107] T. Albrektsson, C. Johansson, Osteoinduction, osteoconduction and osseointegration, *Eur. Spine J.* 10 (Suppl. 2) (2001) S96–101, <http://dx.doi.org/10.1007/s005860100282>.
- [108] B.-S. Chang, Choon-Ki Lee, K.-S. Hong, H.-J. Youn, H.-S. Ryu, S.-S. Chung, K.-W. Park, Osteoconduction at porous hydroxyapatite with various pore configurations, *Biomaterials* 21 (2000) 1291–1298, [http://dx.doi.org/10.1016/S0142-9612\(00\)00030-2](http://dx.doi.org/10.1016/S0142-9612(00)00030-2).
- [109] R.O. Oreffo, J. Triffitt, Future potentials for using osteogenic stem cells and biomaterials in orthopedics, *Bone* 25 (1999) 5S–9S, [http://dx.doi.org/10.1016/S8756-3282\(99\)00124-6](http://dx.doi.org/10.1016/S8756-3282(99)00124-6).
- [110] P.Y. Huri, B. Arda Ozilgen, D.L. Hutton, W.L. Grayson, Scaffold pore size modulates in vitro osteogenesis of human adipose-derived stem/stromal cells, *Biomed. Mater.* 9 (2014) 45003, <http://dx.doi.org/10.1088/1748-6041/9/4/045003>.
- [111] F. Viti, M. Landini, A. Mezzelani, L. Petecchia, L. Milanese, S. Scaglione, Osteogenic differentiation of MSC through calcium signaling activation: transcriptomics and functional analysis, *PLoS One* 11 (2016), e0148173. <http://dx.doi.org/10.1371/journal.pone.0148173>.
- [112] C.K.F. Chan, C.-C. Chen, C.A. Luppen, J.-B. Kim, A.T. DeBoer, K. Wei, J.A. Helms, C.J. Kuo, D.L. Kraft, I.L. Weissman, Endochondral ossification is required for haematopoietic stem-cell niche formation, *Nature* 457 (2009) 490–494, <http://dx.doi.org/10.1038/nature07547>.
- [113] T. Kitsugi, T. Yamamuro, T. Nakamura, S. Kotani, T. Kokubo, H. Takeuchi, Four calcium phosphate ceramics as bone substitutes for non-weight-bearing, *Biomaterials* 14 (1993) 216–224, [http://dx.doi.org/10.1016/0142-9612\(93\)90026-X](http://dx.doi.org/10.1016/0142-9612(93)90026-X).
- [114] S. Nishiguchi, H. Kato, H. Fujita, H.M. Kim, F. Miyaji, T. Kokubo, T. Nakamura, Enhancement of bone-bonding strengths of titanium alloy implants by alkali and heat treatments, *J. Biomed. Mater. Res.* 48 (1999) 689–696, [http://dx.doi.org/10.1002/\(SICI\)1097-4636\(1999\)48:5<689::AID-JBM13>3.0.CO;2-C](http://dx.doi.org/10.1002/(SICI)1097-4636(1999)48:5<689::AID-JBM13>3.0.CO;2-C).
- [115] P.M. Martins, S. Ribeiro, C. Ribeiro, V. Sencadas, A.C. Gomes, F.M. Gama, S. Lanceros-Méndez, Effect of poling state and morphology of piezoelectric poly(vinylidene fluoride) membranes for skeletal muscle tissue engineering, *RSC Adv.* 3 (2013) 17938, <http://dx.doi.org/10.1039/c3ra43499k>.
- [116] S. Bauer, P. Schmuki, K. von der Mark, J. Park, Engineering biocompatible implant surfaces, *Prog. Mater. Sci.* 58 (2013) 261–326, <http://dx.doi.org/10.1016/j.pmatsci.2012.09.001>.
- [117] K. von der Mark, J. Park, Engineering biocompatible implant surfaces. Part II: cellular recognition of biomaterial surfaces: lessons from cell-matrix interactions, *Prog. Mater. Sci.* (2012) <http://dx.doi.org/10.1016/j.pmatsci.2012.09.002>.
- [118] L. Bacakova, E. Filova, M. Parizek, T. Ruml, V. Svoricik, Modulation of cell adhesion, proliferation and differentiation on materials designed for body implants, *Biotechnol. Adv.* 29 (2011) 739–767, <http://dx.doi.org/10.1016/j.biotechadv.2011.06.004>.